Journal of Chemistry of Goods and Traditional Medicine

J Chem Good Trad Med, Volume 5, Issue 5, 2026 Traditional Medicine

# THE USE OF pH IN THE DIAGNOSIS OF DISEASES

***Ibragim R. Askarov***
Andijan State University Professor of the Department of Chemistry, Doctor of Chemistry, Honored Inventor of Uzbekistan, Chairman of the TABOBAT Academy of Uzbekistan
https://orcid.org/0000-0003-1625-0330
***Obidjon Sh. Abdulloev***
Andijan State University Head of the Department of Chemistry of Natural Compounds and Foods, Doctor of Chemistry (DSc), Professor, Member of the Academy Tabobat of Uzbekistan
https://orcid.org/0000-0003-2289-1273
***Barno I. Xolmirzaeva***
"Oltin Vodiy Tabiati" Clinic Specialist
https://orcid.org/0009-0002-9888-4491

DOI: https://doi.org/10.55475/jcgtm/vol5.iss5.2026.760

**Keywords:** pH homeostasis; extracellular acidosis; electrochemical sensor; optical sensor; $^{31}$P MRS; acidoCEST MRI; hyperpolarized MRI; tumor microenvironment; cancer diagnosis; pH-responsive drug carrier.

**Annotation**

**Objective.** To assess technologies for measuring pH in organs and tissues, the relationship of local and systemic acid–base changes to disease, and their clinical translation into cancer diagnosis and treatment.

**Methods.** A narrative synthesis combined targeted literature searches prioritizing studies published in 2016–2026, foundational sources, DOI-based bibliographic checks, and evidence extraction from primary reports. The core corpus reviewed through 1 November 2026 comprised 163 unique articles. Europe PMC records linked to PubMed, Crossref, publisher websites, and electronic scholarly sources were consulted; Consensus supported supplementary searches and identification of relevant source sections. Intracellular, extracellular, organellar, luminal, and biofluid pH were considered separately. A bounded systematic module examined human studies published from 1 January 2016 through 3 November 2026 that quantified tumor extracellular pH using exogenous CEST MRI.

**Results.** Relevant full-text sections were verified for 90 core sources; reliance on abstracts, selected excerpts, or a preprint was recorded for the remainder. Electrochemical and optical sensors support continuous local measurements, whereas $^{31}$P MRS and CEST provide spatial information; their outputs are not interchangeable. Tumor acidosis is associated with metabolic, immune, and membrane processes. Clinical diagnostic studies remain limited by small samples, heterogeneous probe delivery, and inadequate independent reference measurements. Most pH-directed anticancer approaches remain preclinical or in early clinical trials. Correcting acid–base biomarkers can improve selected clinical outcomes, although survival benefits have not been consistent. The systematic module screened 83 unique records and included two clinical reports. These demonstrated the feasibility of $pH_e$ mapping and its promise as a diagnostic biomarker, but provided insufficient data to estimate patient-level sensitivity and specificity.

**Conclusion.** The clinical value of pH depends on the biological compartment, its spatial and temporal variation, and measurement calibration. Priorities include compartment-specific monitoring, multicenter diagnostic validation against independent references, and trials linking biomarker changes to outcomes that matter to patients.

**How to Cite**

Askarov, I. R., Abdulloyev, O. S., & Xolmirzayeva, B. I. THE USE OF pH IN THE DIAGNOSIS OF DISEASES. *Journal of Chemistry of Goods and Traditional Medicine*, *5*(5). https://doi.org/10.55475/jcgtm/vol5.iss5.2026.760

## 1 Introduction

Proton activity influences enzymatic reactions, membrane transport, and protein signaling. Clinical acid–base assessment generally relies on blood measurements, which may differ from conditions in interstitial fluid, the cytosol, and organellar microdomains. Extracellular acidification alongside relatively alkaline intracellular pH is a well-studied example in cancer biology [1, 2, 3]. Measuring local pH over space and time can reveal metabolic activity; whether that signal identifies a particular disease requires separate validation.

Over the past decade, advances have centered on miniaturized, stable proton-sensitive electrodes and optical materials [4, 5, 6], pH-sensitive imaging with CEST, $^{31}$P spectroscopy, and hyperpolarized substrates [7, 8, 9, 10], and the use of tumor acidity to activate molecular probes, control drug release, or provide a therapeutic target [11, 12, 13, 14, 15, 16, 17, 18]. Analytical sensitivity in phantoms, biological responses in animals, and clinical benefit in patients represent successive stages of evidence.

Comparisons across studies are difficult because technologies interrogate different compartments and use different validation criteria. Tumor $pH_e$ estimated with an exogenous CEST agent is distinct from an endogenous amine-CEST signal or $pH_i$-sensitive $^{31}$P MRS [10, 19]. Counting voxels, tissue sections, or cells as independent patients overstates precision [8, 18, 20]. In intervention studies, changes in pH or $HCO_3^-$ do not consistently track tumor control, physical function, or mortality [21, 22, 23, 24].

This review compares the analytical properties of pH measurement methods, interprets organ-specific pathological changes in their biological context, and assesses the clinical maturity of oncological applications. The central questions concern the compartment measured, calibration and reference methods, replication in independent cohorts, and the effect of pH-directed interventions on clinical outcomes.

## 2 Literature search and synthesis methods

The main search window was 1 January 2016 to 1 November 2026, with earlier foundational studies included separately. Thirty-two targeted Europe PMC queries returned 857 records; removal of 52 exact duplicates left 805 unique candidates. From these, 163 journal articles covering measurement methods, organs, and oncology were selected. Seventy-eight were published in 2024–2026 and five before 2016. Not all result pages were retrieved for this broad corpus, so the overall review remains narrative. A bounded systematic module with a separately documented search and eligibility criteria was added; this does not make the entire 163-source corpus a systematic review.

Search blocks combined “hydrogen-ion concentration/pH,” “intracellular/extracellular,” organ and disease names, and terms including “sensor,” “fluorescence,” “magnetic resonance spectroscopy,” “CEST,” “hyperpolarized,” “tumor microenvironment,” “diagnosis,” and “therapy” using Boolean operators. Europe PMC records linked to PubMed and their abstracts were reviewed. DOI, title, author, and journal metadata were checked against Crossref. Scopus and Web of Science were not searched directly.

Eligible original studies measured pH in an organ or biological compartment, evaluated a pH-sensitive signal, investigated a pH-related disease mechanism, or tested a relevant intervention. Methodological papers, clinical consensus statements, reviews, and meta-analyses provided context. Unrelated reports, exact duplicate publications, and materials with unconfirmed bibliographic identity were not used as evidence. Cellular, animal, human, in silico, and secondary synthesis designs were distinguished.

Relevant full-text sections were initially checked for 29 sources. For the remaining 134 DOIs, publisher links, electronic repositories, Europe PMC XML, Crossref metadata, and OpenAlex locations were searched. Fifty-nine full copies were obtained and relevant sections of one additional full-text webpage were checked. Final published full texts were unavailable for 73 sources, with a preprint found for one further

source. The systematic module additionally verified the clinical methods and results of [32]. Access status for the core 163 sources was consequently recorded as relevant full-text sections for 90, abstracts for 69, abstracts plus selected excerpts for three, and an abstract plus a preprint for one. Obtaining a full copy does not imply that all supplementary materials were reviewed.

Consensus received the corpus and research task for an expanded supplementary search. Its synthesis and excerpts were retained separately. A synthesis citing 100 sources was not counted as a completed audit of 134 DOIs or as 100 new independent studies. For some sources without primary full-text access, Consensus supplied methods or results excerpts; these were not labeled as full-text reviews. Reference markers denote access: F, relevant full-text sections; C, abstract plus selected excerpts; A, abstract; and A/P, abstract plus a preprint whose equivalence to the final publication was not fully established. These markers do not rate study quality.

Findings were compared by compartment, technology, calibration range, independent sampling unit, control group, and outcome. Primary reports were preferred for original results, and meta-analyses and subgroup reanalyses were linked to their underlying cohorts. RoB 2 and SYRCLE were not formally applied to the broad corpus. For the diagnostic module, QUADAS-3 eligibility was assessed and an adapted evidence profile based on GRADE domains was developed for biomarker differences. Two independent human reviewers did not conduct separate screening. Associations were distinguished from causation and statistical significance from clinical importance. No new meta-analysis was conducted because independent clinical estimates suitable for pooling were insufficient, rather than because individual patient data were unavailable.

Abbreviations. MRI, magnetic resonance imaging; MRS, magnetic resonance spectroscopy; MRSI, magnetic resonance spectroscopic imaging; CEST, chemical exchange saturation transfer; APT, amide proton transfer; RMSE, root mean square error; MAE, mean absolute error; ROI, region of interest; HCM, hypertrophic cardiomyopathy; DFU, diabetic foot ulcer; HNSCC, head and neck squamous cell carcinoma; RRT, renal replacement therapy; IPD, individual participant data; eGFR, estimated glomerular filtration rate; AUC, area under the receiver operating characteristic curve; ASL, airway surface liquid.

2.1 Systematic module question and eligibility criteria

The question was whether quantitative mapping of extracellular pH in adult human solid tumors using CEST MRI with an exogenous iodinated agent provides evidence for distinguishing malignant from benign lesions. The primary outcome was patient-level diagnostic accuracy against an independent reference diagnosis. Secondary outcomes were between-group $pH_e$ differences, mapping feasibility, and uninterpretable measurements. Histopathology or an appropriate clinical reference can establish disease status without independently establishing the analytical accuracy of the pH measurement.

Original clinical reports had to provide a numerical in vivo $pH_e$ estimate for a human solid tumor or describe an attempt to obtain one. Lack of a control group did not preclude inclusion in the feasibility synthesis. Reports limited to animals, cells, or phantoms; nononcological studies; reviews and methods chapters; protocols without results; and endogenous APT/amine-CEST measurements not converted to absolute $pH_e$ were excluded. The module therefore does not encompass all clinical evidence for $^{31}P$ MRS, deepCEST, or pH-activated surgical fluorescence, which remain within the narrative review.

2.2 Search and assessment procedures

The Europe PMC index, including PubMed-linked records, was searched in title and abstract fields on 3 November 2026. PubMed was not counted as a separate second database. One query covered acidoCEST and iodinated CEST agents; the other combined extracellular pH/tumor acidity/acidosis, CEST, and patient/clinical/human terms. The publication window was 2016-01-01–2026-11-03, without a language filter. All records returned by both queries were retrieved and deduplicated by DOI or, if absent, source and identifier. Complete queries, counts, and selection reasons are provided in the electronic supplement. PRISMA 2020 principles guided transparent reporting of the selection flow [164].

Screening and data extraction were assisted by ChatGPT and do not represent screening or agreement by two independent human reviewers. The protocol was not preregistered. Extracted fields included participant numbers, tumor type, agent, field strength, calibration range, reference method, independent unit

of analysis, failed measurements, and information needed to assess accuracy. Patients, lesions, and voxels were counted separately. Reports excluded after examination of relevant full-text sections are listed with reasons in the electronic supplement.

QUADAS-3 v1.2 requires a numerical diagnostic accuracy estimate as the unit of assessment [165]. The reports were first checked for eligible sensitivity, specificity, or another accuracy estimate. Where none was available, no formal overall QUADAS-3 risk judgment was assigned; a methodological audit organized around its four domains was presented instead. RoB 2 and SYRCLE were not appropriate for the selected clinical observational question. The five GRADE domains were adapted to between-group biomarker differences [166]; the resulting profile is not a formal GRADE assessment of diagnostic accuracy.

3 pH homeostasis and biological compartments

pH is a logarithmic measure of proton activity and has no concentration unit. Buffers, the $CO_2/HCO_3^-$ system, metabolism, and membrane transport of protons and bicarbonate jointly determine local conditions. NHE1, monocarboxylate transporters, carbonic anhydrases, and related systems maintain pH while influencing signaling and metabolic adaptation [1, 2, 3]. A single “organ pH” therefore inadequately defines most biological or clinical questions.

Blood pH, intracellular pH ($pH_i$), extracellular pH ($pH_e$), organellar pH, and luminal fluid pH are distinct quantities. Urine pH is not renal parenchymal pH; exhaled breath condensate pH is not bronchial ASL pH; and gastric luminal pH is not mucosal cell pH [25, 26, 27, 28]. Using a biofluid or isolated specimen as a direct indicator of tissue pH requires validation in the relevant compartment and measurement conditions.

Elevated $pH_i$ in glioma can coexist with reduced $pH_e$ in other tumors. Proton extrusion can help maintain a relatively alkaline cytosol while promoting extracellular proton accumulation [1, 3, 10]. Changes in Golgi or lysosomal pH have distinct biological roles [11, 29]. Therapeutic targets should therefore specify the cell and compartment, timing, and magnitude of the intended change. Figure 5B of the CLC3 study was replaced in a correction; the authors stated that the overall conclusion was unchanged (correction DOI: 10.1038/s41420-026-03008-y).

Buffer capacity and proton transport must be distinguished. The same proton flux can produce different pH shifts in different buffers, and measured pH does not directly indicate the rate of acid production. $CO_2$ diffusion, conversion to $HCO_3^-$, blood flow, and oxygen supply influence local acid clearance. Stable blood values consequently do not establish stability in tissue microdomains [1, 2, 3].

Treating pH solely as a metabolic consequence overlooks its signaling role. Structural and functional studies of Gαi identified pH-responsive states using molecular and mutational approaches [30]. These results support an effect of cytosolic proton activity on protein function, but isolated protein and cell experiments cannot establish organ-level diagnostic thresholds. Assessment of homeostasis should include pH-responsive molecular targets as well as ion transport.

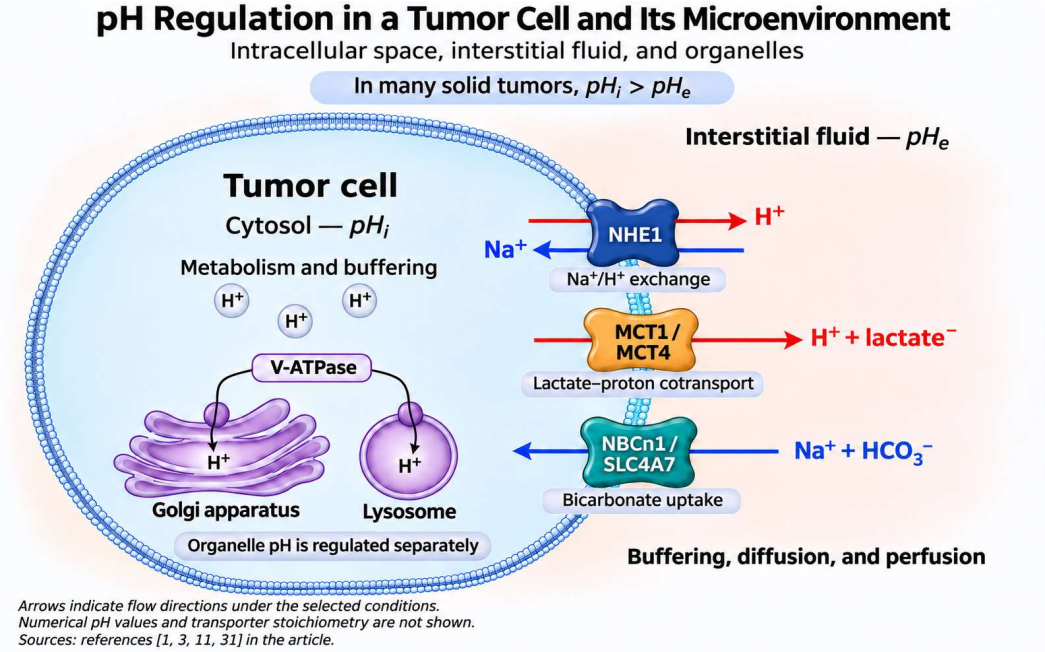



Figure 1. pH compartments in a tumor cell and its microenvironment. Proton/lactate transport and bicarbonate influx contribute to the cytosol–extracellular gradient. Organellar pH homeostasis is regulated separately. The schematic was developed from [1, 3, 11, 31]; arrows simplify transport directions under the selected conditions.

Table 1. pH findings illustrating the limits of direct comparison

| Sample and conditions | Measured value | Interpretation and limits |
|---|---|---|
| Human glioma, 12 patients; 7 T $^{31}$P MRSI; $pH_i$ [10] | Whole tumor 7.057 ± 0.024; normal-appearing white matter 7.006 ± 0.012; $p < 0.001$ | Published means differ by 0.051. This arithmetic difference is not a new effect estimate or individual diagnostic threshold. |
| Human liver tumors; dual-power ioversol CEST; $pH_e$ [7] | 15 carcinomas: 6.66 ± 0.19; 5 hemangiomas: 7.34 ± 0.09; mean ± SD | Small, different diagnostic groups. The benign mean exceeds the reported calibration range of 6.0–7.2. |
| Clinical acidoCEST pilot, two patients [32] | Ovarian tumor $pH_e$ 6.58; inadequate agent in breast tumor | One successful mapping case establishes neither a reference interval nor sensitivity. |
| Rat kidney, n = 5; iopamidol CEST [25] | Cortex 7.0 ± 0.1; medulla 6.8 ± 0.1; calyx 6.5 ± 0.2 | Within-organ gradient. Agent-accessible regions do not define normal human cytosolic pH. |
| Mouse ureteral obstruction; DCE-CEST [33] | Contralateral kidney 6.67 ± 0.08; obstructed kidney 6.79 ± 0.11 | Altered local excretion and perfusion; systemic acidemia cannot be inferred. |
| Infected pig wound, day 13 [34] | Negative pressure: 7.23 ± 0.19; gauze: 7.77 ± 0.23 | Animal wound-surface result, not a treatment threshold for human diabetic wounds. |

Note. SD is specified only where confirmed by the source; other ± values retain the original reporting convention. This table is not a normative atlas. Values from different compartments and methods were not averaged.

4 pH measurement technologies and interpretation

pH sensitivity, agreement with absolute pH, repeatability, and spatial resolution describe different properties. An optical fiber sensor achieved laboratory resolution of 0.0013 pH, drift of 0.003 pH over 22 hours, and a response time below two minutes [5]. These figures do not establish equivalent absolute

accuracy in living tissue, where contact, protein fouling, temperature, and calibration drift require evaluation. Operation of a bioresorbable sensor for more than 100 hours in mice likewise does not validate long-term implantation in humans [4].

Exogenous acidoCEST estimates $pH_e$ from exchangeable protons in a contrast agent. Ratiometric and Bloch-fitting approaches seek to reduce concentration effects, but adequate signal, temperature, $B_0/B_1$ fields, perfusion, and model assumptions remain important [7, 32, 35, 36]. Failed pH estimation in voxels without adequate agent delivery may be informative rather than random: poorly perfused but biologically important regions may be omitted from the map.

Endogenous APT/amine-CEST signals depend on protein content and other exchange components as well as pH. A study showing disagreement between endogenous exchange rate and exogenous acidoCEST $pH_e$ [19], together with the sensitivity of $R_1\rho$ to macromolecular density [37], limits interpretation of CEST signal as absolute pH. These tests need not measure the same biological quantity.

When phosphate components are correctly separated, $^{31}P$ MRSI predominantly estimates $pH_i$ from chemical shifts. The glioma study used 5.7 mL voxels [10], potentially mixing small metabolic regions. In the heart, blood 2,3-diphosphoglycerate complicates phosphate peak separation [38]. Spectroscopy is an important physical reference but is not error-free in every setting.

In the DeepCEST study, 11 of 15 patients contributed to training and four to testing; tumor-region RMSE was approximately 0.04 pH [8]. Comparison of spatially downsampled maps in its Figure 3 yielded RMSE 0.036, $r = 0.45$, and $R^2 = 0.20$. These belong to a different analysis from the development-stage $r = 0.71$ and $R^2 = 0.51$. Low RMSE alone does not demonstrate preservation of biological differences. Estimates for small structures require independent validation because they were learned from a lower-resolution $^{31}P$ reference.

A 2025 Bloch-fitting study examined 120 phantoms and five mice bearing 4T1 tumors. Its abstract described dependence on a 3 μT $B_1$ saturation amplitude, saturation lasting at least one second, iopamidol ≥15 mM, and temperature of 37.0 ± 1.5 °C [36]. These conditions define the demonstrated operating range and cannot automatically be transferred to another probe, temperature, or field strength. A 2026 iobitridol study in 11 rats similarly discussed why PBS phantom calibration should not be transferred to living tissue without considering magnetization-transfer confounding [39].

The 36 000 spectra generated from 200 phantoms can support machine learning but do not constitute 36 000 independent biological samples [40]. Temperature, proteins, perfusion, and motion differ across phantoms, animals, and patients. Phantom regression error, animal agreement with a reference, and clinical discrimination must therefore be evaluated separately [8, 35, 40]. Denoising can improve signal quality [41]; whether smoothing also obscures small acidic regions should be tested against an independent reference. This is a methodological possibility, not a demonstrated error of the algorithm.

Different pH estimates obtained with a nanoscale CEST polymer, a monomeric probe, and iopamidol indicate that probe architecture can affect calibration as well as signal strength [42]. Monitoring enzyme activity and pH with one agent offers functional advantages but requires separation of their contributions to the signal [43, 44]. An independent measurement based on another principle, such as LC–MS assessment of enzyme activity, strengthens interpretation when several biological processes affect one imaging output [43].

Administration route also determines biological coverage. In an orthotopic pancreatic tumor model, intraperitoneal iopamidol arrived later than intravenous agent; the comparison of pH estimates gave $p = 0.16$ [45]. Absence of statistical significance does not establish equivalence without a prespecified margin. Multislice CEST improved coverage of gradients across tumor core, edge, and kidney [46], while still requiring adequate agent delivery and valid calibration in each voxel.

Optical approaches include fluorescence-lifetime-based SypHerRed, membrane-bound pHLuc, and ratiometric chemiluminescent probes [47, 48, 49]. Genetic reporters can monitor cells or cell surfaces in tumor models but are distinct from diagnostic agents ready for patient administration. An enzyme-activated DNA nanosensor sought to localize ischemic injury [50]; activation alone does not establish pH specificity because delivery and enzyme abundance can also affect signal. Dual photoacoustic/NIR-II probes [51] and

EPR profiling [52] extend depth and microenvironmental information, but the reviewed evidence does not support a universal human accuracy estimate for these methods.

The administered precursor is critical in hyperpolarized imaging. Extracellular distribution of bicarbonate differs from intracellular production of $HCO_3^-/CO_2$ from pyruvate [53, 54, 55]. An approach based on alanine ethyl ester transport and metabolism sought to distinguish both compartments [56]. Accounting for bidirectional chemical exchange in pulse sequences can improve signal [57], but a ratio may not reliably represent pH before exchange equilibrium is reached. A study describing clinically translatable $^{13}C$ bicarbonate was performed in animals on a clinical 3 T scanner [58]; this does not constitute validation in patients.

Table 2. Analytical properties and clinical translation of measurement technologies

| Method and physical principle | Strength and evaluated example | Main limitation and validation need |
|---|---|---|
| Electrochemical electrode: proton-dependent potential | Continuous contact-site monitoring; miniaturization for deep tissues [6] | Invasive deep placement, drift, and biofouling. Sweat or wound sensing does not map deep organs [59]. |
| Optical intensity, ratio, or fluorescence lifetime | Local/cellular monitoring; laboratory fiber resolution 0.0013 pH [4, 5, 47] | Scattering, photostability, probe localization, and limited deep-organ access. |
| $^{31}P$ MRS/MRSI: phosphate chemical shift | Endogenous metabolic reference; human glioma and cardiac applications [10, 38] | Low signal, partial volume, mixed Pi peaks; glioma voxel 5.7 mL. |
| Exogenous CEST, including acidoCEST: exchange and ratio/model analysis | $pH_e$ maps; human liver tumors and a clinical pilot [7, 32] | Delivery, concentration, field, and temperature dependence; protocol-specific calibration. |
| Endogenous CEST or $R_1\rho$: exchange-sensitive signal | Metabolic assessment without exogenous contrast [60, 61, 62] | Difficult separation of pH and macromolecules; not equivalent to absolute pH [19, 37]. |
| Hyperpolarized $^{13}C$: $HCO_3^-/CO_2$ ratio or probe shift | Rapid metabolic imaging; Z-OMPD $T_1 \approx 2$ min at 1 T; up to 1.9 ppm/pH [9, 55] | Short signal window, equilibrium, compartment, production, and safety [58, 63]. |
| PET, EPR, and photoacoustic probes | Deep signal or microenvironment profiling; preclinical studies, 2024–2026 [51, 52, 64] | Probe kinetics also affect signal; separate clinical evidence for absolute pH accuracy is needed. |
| Machine-learning CEST analysis | Test MAE 0.054 pH in a 38-mouse study; human DeepCEST test n = 4 [8, 35] | Reference error propagates to the model; voxels are not independent patients. External-center testing is needed. |

Note. No universal accuracy or spatial resolution value is assigned because field strengths, probes, protocols, and specimens differ. Sensitivity in ppm/pH is not itself a pH error. Blood or luminal monitoring and deep tissue imaging also differ in invasiveness.

5 Comparative synthesis by organ and disease

5.1 Renal acid excretion and local pH

Blood bicarbonate, urine pH, ammonium excretion, and renal parenchymal pH represent different aspects of renal acid handling. Urine pH alone does not fully characterize net acid excretion and should be interpreted with ammonium [26]. Distal renal tubular acidosis registries and studies of RhBG connect genetic defects with clinical phenotypes [65, 66, 67], without establishing the mechanism of every local pH imaging change.

Higher CEST pH in an obstructed kidney [33] is compatible with reduced blood bicarbonate in chronic kidney disease. The former concerns local contrast excretion, perfusion, and urinary conditions; the

latter concerns systemic acid–base balance. Ischemia–reperfusion models likewise require joint assessment of pH and perfusion [68, 69]. Before renal CEST can substitute for eGFR, the physiological component to which it responds must be established.

Functional genetic evidence can help interpret these findings. The RhBG study examined CRIC exomes from 507 participants of African and 1147 of European ancestry [67]. An association between a rare variant and disease is distinct from functional evidence that it alters $NH_3/NH_4^+$ transport. The authors noted limitations in rare-variant numbers and sex-stratified analyses. One transporter gene cannot explain urine pH or acidosis severity in every patient.

Clinical outcomes also depend on the achieved intervention effect. The abstract of a pragmatic trial evaluating long-term bicarbonate treatment and quality of life reported no clear improvement and limited attainment of target levels [70]. This is directionally consistent with BiCARB and VALOR-CKD, but their data were not pooled because designs, populations, and outcomes differed [23, 24].

5.2 Gastric and esophageal pH monitoring

Clinical criteria for esophageal pH and impedance monitoring are better established than for many tissue pH technologies, with the Lyon 2.0 consensus providing a framework [71]. Sensor placement, recording duration, and day-to-day variability still affect classification [72, 73, 74]. In a study of 944 examinations, sensitivity of 24-, 48-, and 72-hour recordings was 62.5%, 76.6%, and 88.2%, respectively, against the same recording extended to 96 hours [75]. These are not accuracy estimates against an independent external standard.

The pHoenix Score reduced borderline classifications from 11% to 4.7% in 318 patients [76]. When it and the DeMeester reference use the same pH recording, some agreement may reflect shared input data. The Milan Score AUC of 0.812 describes discrimination of pH-defined gastroesophageal reflux disease by a manometric score, rather than pH sensor accuracy [77]. Interpretation requires identifying both the index test and its reference.

Drug control of gastric luminal pH provides a practical example of local pH pharmacodynamics. A five-period crossover pilot compared proton pump inhibitors in five healthy volunteers [27]. Repeated periods reduce between-person variability but do not increase the independent sample beyond five participants. Intragastric pH differences do not directly establish superior symptom relief, erosion healing, or long-term clinical outcomes.

A 96-hour pilot monitoring saliva and oral biofilm enrolled 12 participants, with 11 completing the study [78]. Food, glucose exposure, and local biofilm generated different trajectories within the same oral cavity. Reclassification of functional heartburn using 24-hour MII-pH [79] likewise shows the importance of recording windows and clinical follow-up. The adult cystic fibrosis study of distal colonic pH reanalyzed previously collected capsule data [80] and was not counted as a new independent cohort.

5.3 pH changes in brain disorders

Acidosis and oxidative stress follow different time courses in ischemic stroke; dynamic rodent observations show the limitations of treating acidity as a single static endpoint [81]. ASIC1a-related injury [82] and protection associated with metabolic acidification and mitophagy in selected Parkinson cell models [83] concern different diseases, time points, and cellular processes. They do not justify generalized acidification of the human brain.

APT and ratiometric CEST can detect stroke-related changes [62, 84], but correlation between CEST methods does not independently validate absolute pH. The corrected traumatic brain injury $^{31}P$ MRS report identified metabolic differences even in areas with limited structural MRI changes [85]. Its corrigendum revised pH medians, selected p values, and tables (DOI: 10.1177/0271678X19853211); quantitative interpretation should use the corrected report. Incremental prognostic value requires testing in an independent clinical cohort.

In a 7 T $^{31}P$ MRS Parkinson study, 19 patients and 19 controls were divided between two metabolic measurement cohorts [86]. Unchanged metabolite ratios do not establish unchanged absolute concentrations

or fluxes. Occipital measurements also cannot be equated with substantia nigra conditions. A cerebrovascular regulation review supports distinguishing arterial and perivascular pH and accounting for $CO_2$ diffusion [87].

The 2025 $^{31}P$ shift analysis in 11 glioma patients reused earlier data, including the 2024 study of 12 patients [10, 88], and is not an independent replication. $Mg^{2+}$ effects on ATP shifts and incomplete age matching of healthy controls introduce confounding beyond pH [88]. Attributing all phosphate spectral differences to proton activity can obscure other ionic features of the tumor microenvironment.

5.4 pH and metabolism in the heart and skeletal muscle

A 7 T $^{31}P$ MRS program involved 12 healthy participants and three patients with HCM; some individuals participated in multiple experiments. Energetic ratios differed in the HCM comparison, whereas $pH_i$ did not ($p = 0.508$) [38]. A neutral result in three patients neither excludes disease nor establishes poor diagnostic sensitivity. The reported pH repeatability coefficient was 0.052, which should not be used as a diagnostic threshold for small mean differences in another organ.

Maintaining acidity during early reperfusion was protective in selected animal models [89, 90]. Cardiomyocyte NHE1 overexpression under hyperglycemia was also associated with protection [91]. Conversely, alkalinization contributed to an arrhythmogenic mechanism in SLC4A3-related human iPSC-derived cardiomyocytes [92]. Interpretation must account for transport fluxes, $Na^+/Ca^{2+}$ balance, disease stage, and compartment. Evidence concerning carnosine and β-alanine in exercising skeletal muscle addresses exercise buffering and should not be transferred directly to resting cardiac pH [93].

The balance of acid-extruding and acid-loading transporters determines cardiomyocyte pH [94]. Reduced NHE1 activity during hypoxia [95] shows that transporter expression alone does not determine activity. Loss of NBCn1 in mice impaired atrial acid extrusion and increased blood pressure and hypertrophy [96]. A global knockout cannot fully separate direct cardiac effects from consequences of hypertension. The published abstract on distinct metabolic effects of intracellular and extracellular acidosis [97] supports compartment-specific interpretation; the available 2022 preprint was not counted as the final journal full text.

5.5 Airway pH and cystic fibrosis

Low ASL pH impaired bacterial killing in newborn cystic fibrosis pigs [98]. In vivo measurements in children did not confirm airway acidification [99], and another pig study also found no difference [100]. Species alone cannot explain discordance within the same animal species. Anatomical site, age, inflammation, paracellular $HCO_3^-$ flux, cellular composition, and sensor conditions are plausible contributors [20, 101, 102, 103].

A dynamic study examined breathing-related nasal pH oscillations in 10 controls and 11 participants with cystic fibrosis [104]. Brief alkaline peaks do not define a stable normal lung pH. Improvement in mucus properties with CFTR modulators was attributed more to hydration than restoration of pH [105], limiting explanations based on pH alone. Nasal, bronchial, and exhaled breath condensate measurements should remain distinct [28, 101].

Mechanistic experiments should distinguish pH from $HCO_3^-$. Manipulation of pH and $HCO_3^-/CO_2$ in newborn pig ASL supported an effect of acidification on mucus viscosity [106], although isolated mucus diffusion does not capture every mechanical component of mucociliary transport. During ivacaftor treatment, mean ASL pH did not change significantly, whereas individual pH shifts correlated with reductions in sweat chloride [107]. Group means and correlations between individual changes address different statistical questions.

SERS microsensors were evaluated in air–liquid interface cultures from six cystic fibrosis and six non-cystic fibrosis donors; selected experiments used smaller donor subsets [108]. The nasal cell study of TMEM16A and SLC26A4 included repeated measurements from three donors [109]. A 2026 comparison of nasal and bronchial proteins analyzed three successfully cultured donors per group [101]. Technical replicates, cells, and donors therefore require separate counts: numerous measurements do not increase donor independence.

WNK inhibition improved ASL pH and defense functions in human-derived cultures [110], without yet establishing reduced infection or improved lung function in patients. An exhaled condensate electrode

study collected repeated samples from two healthy volunteers [28]; this does not establish population reference values. The asthma-related AUC of 0.72 [111] must also be interpreted alongside sampling, temperature, humidity, and pollutant effects [112].

5.6 pH in the liver and wounds

Studies of hepatic stellate cells indicate that perisinusoidal acidity can amplify bile salt effects and link NHE1 and V-ATPase pathways with fibrogenic states [113, 114, 115]. Cell experiments and pantoprazole findings in a DDC mouse model do not establish a standard treatment for human fibrosis [113]. Low $pH_e$ in liver cancer likewise does not provide a validated threshold for every diagnostic setting [7].

A prospective diabetic foot ulcer study included 187 of 235 initial participants and recorded 1531 measurement points [116]. These points are not independent patients. Follow-up was censored for 142 patients, with an unknown reason reported for 136. Wound-bed pH <6.7 distinguished healing within three days with 75.7% sensitivity and 72.7% specificity; wound-edge pH <6.8 yielded 88.0% and 75.8%. Repeated-measure dependence, threshold selection within the same cohort, and extensive censoring limit generalization without external validation. A higher threshold predicting entry into the proliferative phase concerns a different outcome and need not conflict with the healing findings.

A review of hepatic $Na^+/H^+$ exchange distinguishes hepatocyte, cholangiocyte, and stellate cell functions [117]. Biliary, cytosolic, and perisinusoidal measurements should therefore not be combined into one liver pH value. Deep Image Prior reconstruction was investigated in 49 rabbits, but a high-resolution reference was obtained in only two [118]. The larger total sample does not remove the limitation of a small reference dataset.

The 3 T acidoCEST-UTE approach was adapted to short-$T_2$ cartilage and meniscus [119]. Associations between acidity and osteoarthritis symptoms [120] require separation from inflammation, perfusion, and degeneration. A correction to the osteoarthritis article revised its pH color scale; interpretation here uses the corrected 6.5–8 range (correction DOI: 10.3390/ijms241512346).

An association between lower pH and wound healing does not establish the efficacy of a particular treatment. Of four diabetic foot ulcers treated with Trigona honey, two healed and two remained unhealed at eight weeks [121]. Without controls, differences in severity and concurrent care prevent attribution to honey or pH alone. In the pig NPWT study, wound pH and bacterial burden changed together [34], but perfusion and mechanical effects also occurred. A causal mediating role for pH requires separate analysis.

Table 3. Organ-specific evidence and its interpretation

| Organ or specimen | Principal evidence | Supported interpretation and remaining question |
|---|---|---|
| Kidney | Urine pH and ammonium; local CEST; clinical RCTs [23, 26, 33] | Acid excretion, local pH, and progression are separate outcomes; biomarkers are not fully interchangeable. |
| Esophagus/gastric lumen | Ambulatory monitoring and consensus [27, 71, 75, 76] | Established diagnostic use; duration and reference selection affect accuracy. |
| Brain | Stroke dynamics and CEST/MRS [62, 81, 84, 85] | Metabolic information is available; not every signal change represents absolute pH. |
| Heart/muscle | Neutral HCM pH with altered energetics; reperfusion timing [38, 89, 90, 93] | pH is not a universal disease marker. Transient and chronic acidosis differ. |
| Airway surface | Discordant static cystic fibrosis findings and dynamic oscillations [98, 99, 100, 104] | Microdomain and temporal standardization are needed; uniform acidosis across all ages is unproven. |
| Liver | Hepatic stellate cell mechanisms and a human tumor CEST pilot [7, 113, 115] | Fibrosis mechanisms and diagnostic cancer classification require different evidence. |
| Wound | Prospective DFU observations and a pig intervention [34, 116] | pH may monitor healing; observations alone do not establish a causal treatment target. |

6 pH regulation and biological effects in the tumor microenvironment

Aerobic glycolysis, proton extrusion, $CO_2$ hydration, perfusion, and buffering jointly shape tumor $pH_e$ [1, 3]. Strong lactate–pH correlations in selected models [21] do not establish a common acid source or causal pathway in every tumor. A 2025 CRISPR study identified ERK signaling and mitochondrial respiratory adaptation to acidosis [122], showing that acidic tumors are not simply collections of glycolysis-dependent cells.

Acidity also affects processes beyond central metabolism. Increased fatty acid uptake in breast and pancreatic cancer cells [123], glycocalyx remodeling in glioblastoma [124], and injury to liver-resident NK cells in colorectal metastases [125] connect the microenvironment with nutrient uptake, membrane properties, and immune surveillance. A mechanism demonstrated in cells or mice does not automatically establish an independent predictor of invasion, metastasis, or treatment response in patients.

Ferroptosis studies illustrate the importance of compartment. Reducing extracellular acidosis may support immunity, whereas disrupting Golgi or other organellar pH can reduce cancer cell viability [11, 31, 126]. In the TMEM87A study, altered Golgi pH homeostasis affected ferroptosis sensitivity [11]. These directions concern different targets and cannot be reduced to a general claim that acidity is harmful and alkalinity beneficial.

Tumor acidosis is better understood as part of a feedback system than as either an initiating cause or a passive by-product. Reviews connect pH transport with the Warburg phenotype [1, 3, 127]; mathematical models show that different combinations of $CO_2/HCO_3^-$, oxygen, and metabolic fluxes can yield similar pH [128]. A modeled 6.7–7.4 range is not a measured human reference interval. Model parameters also require independent experimental validation.

An inverse association between $pH_e$ and GLUT1 in mouse myeloma bone marrow links acidosis with metabolic phenotype [129]. Comparisons of 4T1 and 67NR tumors associated acidic spatial heterogeneity with aggressiveness [130]. Bilateral tumors in one animal do not constitute independent animals. Genetic and functional evidence for the dysadherin–CA9 pathway in colorectal cancer strengthens the molecular basis of acid adaptation [131], while expression associations, knockout effects, and clinical therapeutic benefit remain distinct evidence levels.

T-cell dysfunction, regulatory T-cell adaptation, and myeloid responses differ under the same pH conditions [132, 133]. Whole-tumor pH alone therefore offers limited prediction of immune effects. A review of compartment-directed strategies emphasizes joint measurement of delivery, cell death, and immune activity when modifying pH [134]. These criteria provide a framework for comparing emerging ferroptosis and immunotherapy platforms.

Table 4. Evidence connecting pH with cancer mechanisms

| Direction and model | Main finding | Comparative significance |
|---|---|---|
| Human glioma, $^{31}P$ MRSI [10] | Higher $pH_i$; Ki-67 association $r_s = 0.78$, $p = 0.001$ | Association with proliferation, not causation or independent diagnostic accuracy. |
| Breast/pancreatic cells [123] | Acidosis increased lipid uptake | Low pH modifies nutrient handling beyond glycolytic adaptation. |
| Experimental glioblastoma [124] | Glycocalyx remodeling, lipid uptake, and ferroptosis effects | Cell-surface composition can alter responses to the same pH. |
| Colorectal liver metastasis, human material and experiments [125] | Acidification associated with NK-cell apoptosis | Immunosuppressive mechanism; clinical neutralization benefit needs testing. |
| TMEM87A, cells and mice [11] | Golgi pH maintenance contributed to ferroptosis resistance | Organellar and extracellular pH require separate assessment. |

| Direction and model | Main finding | Comparative significance |
|---|---|---|
| SLC4A7, NSCLC models [31] | Intracellular acidification and extracellular alkalinization associated with immune responses | Dual-compartment strategy; clinical efficacy remains unestablished. |
| Syrosingopine, cells and mice [135] | Cellular effects did not yield significant in vivo $pH_e$ or primary growth differences | Target inhibition does not always change the microenvironment or tumor outcome. |

7 Clinical evidence for pH-based cancer diagnosis

Human exogenous CEST studies demonstrate that tumor acidity can be measured, although small pilots do not establish a clinically validated classifier [7, 32]. The liver study separated group means of 6.66 and 7.34, but reported a calibration range of pH 6.0–7.2 [7]. The benign-group estimate exceeds that range. This raises uncertainty concerning extrapolation and measurement validity; it does not invalidate the finding. No threshold or AUC was constructed from these two means.

The first ONM-100 study in 30 patients detected all nine positive surgical margins [18]. This is not an overall accuracy of 100%: margin specificity was 75% in breast cancer and 57% in HNSCC. The AUC of 0.9875 concerns 59 tissue sections from 15 dose-expansion patients, rather than 59 independent patients. Full-text assessment confirmed that the subsequent 13-patient HNSCC report reanalyzed the same NTR7085/EudraCT 2017-003543-38 program [136]; participant counts were not added across reports.

An encouraging early lung tumor fluorescence report [16] should be considered alongside the subsequent 20-patient phase II study, which reported 31.6% sensitivity and 33.3% specificity [15]. These findings retain the biological rationale but show inadequate diagnostic performance for that protocol. In the peritoneal metastasis study, residual disease was detected in 20 of 40 evaluable patients [17]. The resulting 50% is a detection proportion, not diagnostic sensitivity.

Preclinical pH-based discrimination does not establish a universal marker separating cancer from inflammation. One lung study compared adenocarcinoma in seven male mice with fungal granulomas in five female mice, with additional differences in age and disease duration [137]. This design cannot fully separate malignancy-related pH effects from group composition. Ioversol maps in breast and liver models likewise do not directly establish human diagnostic accuracy [138].

The pancreatic cancer–pancreatitis model illustrates another distinction: $pH_e$ differentiated established cancer from inflammation but did not predict which pancreatitis would progress to cancer rather than resolve [139]. Differential diagnosis and future-risk prediction are separate tasks. Combining FDG PET and CEST adds information on glucose uptake and acidosis [140], while pH-sensitive PET substrates provide further possibilities [64]. Standard FDG uptake is not a pH measurement, and accumulation of a pH-activated substrate can still depend on pharmacokinetics.

In a hyperpolarized prostate model, minimum voxel $pH_e$ correlated strongly with maximum lactate/pyruvate ratio, whereas correlations of tumor means were not statistically significant [141]. Minima, maxima, and means capture different features. Selecting the statistical unit after inspecting favorable results risks bias; future protocols should prespecify the principal spatial biomarker.

Table 5. Clinical diagnostic studies and units of analysis

| Study and design | Quantitative result | Clinical validation limits |
|---|---|---|
| AcidoCEST, two-patient translational pilot [32] | $pH_e$ 6.58 in one tumor case; inadequate contrast in the other | Feasibility; sensitivity/specificity not established. |
| Liver CEST, 15 + 5 patients [7] | Carcinoma 6.66 ± 0.19; hemangioma 7.34 ± 0.09 | $B_1$, motion, low SNR, and high estimates beyond calibration. |
| Glioma $^{31}$P MRSI, n = 12 [10] | $pH_i$ and Ki-67: $r_s = 0.78$; $p = 0.001$ | Correlation, not an external classifier test or AUC. |
| DeepCEST, n = 15; test n = 4 [8] | Tumor ROI RMSE ≈0.04 pH | Model–reference agreement, not independent clinical-outcome validation. |

| Study and design | Quantitative result | Clinical validation limits |
|---|---|---|
| ONM-100, phase I, n = 30 [18] | Positive margins 9/9; AUC 0.9875 from 59 sections in 15 patients | Small sample and correlated sections; patient-level external validation needed. |
| HNSCC reanalysis, n = 13 [136] | Positive margins 6/6; TBR >1.5 | Same program as [18], not independent replication. |
| Pegsitacianine, lung phase II, n = 20 [15] | 6/19 malignant lesions fluorescent: 31.6%; specificity 33.3% in 3 benign lesions; PPV 75%; NPV 7.1% | Very few benign lesions; patients and lesions must be counted separately. |
| Pegsitacianine, peritoneal phase II [17] | 50 enrolled, 40 evaluable; residual disease in 20/40 | Uncontrolled additional detection; recurrence or survival benefit not established. |

Diagnostic validation should establish measurement validity, discrimination of disease, and improvement in clinical decisions. The reviewed studies address different stages of this sequence. A pH-sensitive fluorescent focus is not an absolute pH map, and obtaining a map does not itself establish a beneficial surgical or treatment decision [7, 8, 15, 18].

7.1 Systematic analysis of exogenous CEST MRI $pH_e$ mapping

The two queries returned 62 and 32 records. Removing 11 duplicates from 94 records left 83 unique records for screening. Seventy-seven were excluded by title and abstract; relevant full-text sections were examined for six reports. Four were excluded because they presented only animal or laboratory data, leaving two independent clinical reports [7, 32]. These counts concern the bounded module and were not combined with the narrative corpus of 805 candidates and 163 selected sources.

Table 6. Clinical reports quantifying human tumor $pH_e$ with exogenous iodinated CEST MRI

| Report and unit of analysis | Measurement and calibration | Result and diagnostic interpretation |
|---|---|---|
| Jones et al., 2017 [32]. Two patients: breast cancer and ovarian cancer metastases. Three metastatic lesions belonged to one patient. | 3 T; iopamidol; Bloch fitting. Clinical maps restricted to pH 6.2–7.0. | Mean metastatic $pH_e$ 6.58; most reliable mapping in the well-enhanced lesion. Inadequate breast tumor delivery prevented reliable mapping. Diagnostic sensitivity cannot be calculated from these two cases. |
| Tang et al., 2020 [7]. Results table: 15 liver carcinoma and 5 hemangioma patients. | 3 T; ioversol; dual-RF-power ratio. Reported phantom range pH 6.0–7.2. | Carcinoma $pH_e$ 6.66 ± 0.19; hemangioma 7.34 ± 0.09. Promising separation, but benign estimates exceed calibration. Three images were excluded; their relationship to initial and final counts was incompletely clarified. |

Note. The ± values denote standard deviations as reported in the sources. These results are not pooled effects. In the liver comparison, 6.66 − 7.34 = −0.68 pH units is an arithmetic difference between published means, not a diagnostic threshold or patient-level classification accuracy. The proportion of technically successful maps also differs from disease-detection sensitivity.

7.2 Diagnostic accuracy and methodological audit

Neither included report provided a complete patient-level 2 × 2 table of true positives, false positives, true negatives, and false negatives, or alternative information sufficient to reconstruct accuracy for this question. No universal pH threshold had been externally validated. Sensitivity, specificity, and AUC were therefore not reconstructed, and mean/SD data were not used to simulate ROC curves. Because the numerical accuracy-estimate requirement of QUADAS-3 was not met, Table 7 is a domain-based methodological audit rather than a formal QUADAS-3 assessment [165].

Table 7. Methodological factors affecting clinical interpretation

| Domain | Jones et al. [32] | Tang et al. [7] |
|---|---|---|
| Participants | Confirmed malignant cases without benign controls; not a consecutive diagnostic cohort. | Two prediagnosed groups; applicability to all indeterminate liver lesions is limited. |
| Index test | Agent distribution and map-range restriction affect results. | Estimates beyond calibration; $B_1$ homogeneity not evaluated. |
| Target condition and reference | Histology establishes tumor diagnosis, not independent tissue pH. | Histologically confirmed carcinoma; hemangioma reference and blinding inadequately described. |
| Analysis | Three lesions cannot be counted as three independent patients. | Group-specific flow of excluded images is unclear. |
| Availability of accuracy estimates | No patient-level accuracy estimate; no formal overall QUADAS-3 judgment. | No patient-level accuracy estimate; no formal overall QUADAS-3 judgment. |

7.3 Certainty of evidence and feasibility of meta-analysis

Between-group differences in measured $pH_e$ and correct classification of individual patients are separate questions. The liver comparison addresses the first, while no eligible numerical accuracy estimate addresses the second. Table 8 therefore adapts GRADE to an observational biomarker comparison. It does not rate diagnostic accuracy, all organ-specific cancers, or the overall value of pH-based diagnosis [166].

Table 8. Adapted GRADE profile for the $pH_e$ difference between liver carcinoma and hemangioma

| Assessment component | Rationale and decision | Effect on certainty |
|---|---|---|
| Starting level | Observational between-group biomarker comparison; results table n = 20. | Started at low certainty. |
| Risk of bias | Calibration and exclusions affect credibility of the measured difference. | Serious; downgraded one level. |
| Consistency | No second independent cohort repeated the same clinical comparison. | Not assessable; consistency unconfirmed. |
| Indirectness | Two selected diagnoses in one organ do not represent all suspicious solid lesions. | Serious limitations on broad diagnostic application. |
| Imprecision | No independent validation or CI for the group difference. Small n alone was not a separate downgrade criterion. | No additional number of downgrade levels assigned. |
| Publication bias | One eligible comparison does not permit statistical assessment. | Absence of bias was not assumed. |
| Upgrading | Large separation not independently confirmed free of measurement/selection problems. | No upgrading. |
| Final profile | Limited confidence in generalizable magnitude of the biomarker difference. | Very low. No sensitivity/specificity certainty rating. |

The two reports do not provide two compatible diagnostic effects: one describes clinical feasibility and the other compares groups of liver tumors. Only one eligible clinical $pH_e$ comparison was available, with no poolable accuracy estimates. No meta-analysis, $I^2$ statistic, funnel plot, or statistical publication-bias test was performed. Lack of individual patient data is not presented as a general barrier to aggregate-data meta-analysis.

7.4 Clinical and research implications

This synthesis shows that spatial assessment of human tumor $pH_e$ has reached the clinical setting. Quantitative mapping at 3 T offers a basis for adding metabolic microenvironment information to anatomical

imaging. The strongest opportunity lies in organ-specific functional biomarkers addressing defined clinical questions. Observed group separation supports prospective validation; individual-patient value remains to be established externally.

A subsequent diagnostic trial should enroll consecutive patients with uncertain diagnoses, use a consistent clinical reference, prespecify the pH threshold, and interpret images blinded to the reference. Lesions without adequate agent delivery should be reported as technical failures. A model incorporating pH should be compared with standard MRI at the patient level to measure incremental diagnostic value and effects on decisions.

The module is limited by one primary index, the absence of a complete registry for supplementary web searches, no preregistered protocol, and no two independent human reviewers. Eligible studies outside the search scope may have been missed. The methodological audit and adapted GRADE profile were not independently repeated by human experts. Conclusions apply to the specified technology and period.

8 pH-directed treatment and clinical translation

pH-responsive drug carriers, proton-transport inhibitors, and microenvironmental buffering act differently. Carriers use acidity to trigger release; inhibitors disrupt cellular pH regulation; buffers alter extracellular conditions [3, 142, 143]. Each approach requires evidence of delivery, compartment-specific target effects, toxicity, and tumor control.

A 2026 erdafitinib liposome released 49% of its payload within one hour at pH 5.3 [12]. This condition differs from extracellular tumor pH of 6.5 and may better match endosomal or lysosomal activation, although localization must be demonstrated. Preclinical results for the formulation should not be conflated with existing clinical use of the erdafitinib molecule to imply that the new formulation is approved.

Buffering or transport targeting combined with immunotherapy has produced favorable experimental results [31, 126, 144, 145, 146]. Esomeprazole sensitization nevertheless improved outcomes in 4T1 tumors and worsened them in B16-F10 [147]. Lansoprazole and amiloride showed discordant cellular and mouse effects [148], and syrosingopine-mediated MCT inhibition did not produce the expected in vivo changes [135]. Drug class and pH effects alone do not establish universal anticancer efficacy.

The AZD3965 phase I study evaluated dose and safety in 40 patients, with seven dose-limiting toxicities [13]. In the 17-patient SLC-0111 phase I trial, there were no objective responses; two patients had stable disease for more than 24 weeks [14]. These studies demonstrate the feasibility of targeting these pathways in humans, but uncontrolled stabilization does not establish efficacy or survival benefit. Evidence for these experimental systems is insufficient to support routine oncology use; no comprehensive regulatory-approval audit was conducted.

The dichloroacetate study illustrates the distinction between metabolic monitoring and efficacy. After three days, TS/A tumor $pH_e$ changed by $+0.10 \pm 0.03$ in treated animals and $-0.12 \pm 0.03$ in controls; metabolic separation diminished by day 15 [21]. No reliable tumor-growth or survival benefit was demonstrated. An early metabolic response can inform resistance monitoring without substituting for treatment benefit.

In a foundational mouse bicarbonate study, $pH_e$ increased without a change in $pH_i$, and selected metastatic outcomes improved; the B16 model did not benefit [149]. A subsequent immunotherapy combination study reported favorable results [146]; the origin of its Panc02 cell line was corrected (DOI: 10.1158/0008-5472.CAN-17-0559). These findings support investigation of extracellular buffering without establishing that systemic alkalinization treats cancer in patients.

Some platforms combine local acidification with extracellular neutralization. Nanocatalytic ferroptosis [150], Lipiodol Pickering emulsions for embolization [151], and spatial electrochemical control using Fe/Pt electrodes [152] seek to injure tumor cells while modifying the immune environment. Their pharmacology differs from that of an oral buffer. An MRI-trackable tumor-acidifying nanoplatform [153] further shows that location, duration, and accompanying chemistry matter alongside the direction of pH change.

Gastrointestinal transit and target delivery are major translational issues for oral colorectal nanogels [154]; retention and endocytosis are important for intravesical liposomes [12]. Reviews describe release through bond cleavage, protonation, or charge changes [142, 143]. Each formulation requires control formulations, stability in physiological protein conditions, release kinetics, and drug-exposure measurements before pH responsiveness can be related to efficacy.

Table 9. Comparison of therapeutic strategies

| Strategy and stage | Evidence and biological target | Unresolved issue |
|---|---|---|
| pH-responsive liposomes, nanogels, and peptides; preclinical [12, 154, 155] | Release/activation in local or organellar acidity | Human pharmacokinetics, immunogenicity, repeat dosing, and relevant pH range. |
| L-DOS47; pancreatic mouse model [144] | Mean $pH_e$ increase +0.13; enhanced anti-PD1 response | Clinical meaning of a small shift and target engagement in patients. |
| Transdermal bicarbonate; bladder cancer mouse model [126] | Intratumoral pH and immune responses | Human efficacy, local/systemic safety, and duration unknown. |
| PPI, amiloride, or syrosingopine; experimental [135, 147, 148] | Altered proton or lactate/proton transport | In vitro–in vivo discordance and tumor-model dependence. |
| AZD3965, MCT1 inhibitor; clinical phase I [13] | 40 patients; recommended phase II dose 10 mg twice daily | Dose-limiting toxicity; not controlled evidence of efficacy. |
| SLC-0111, CAIX inhibitor; clinical phase I [14] | 17 patients; 0 objective responses; two prolonged stabilizations | Small uncontrolled trial; pH pharmacodynamics incompletely demonstrated. |
| Dual-compartment ferroptosis/immune strategies; preclinical [11, 31, 150, 151, 152] | Selective modification of extracellular, cytosolic, or organellar pH | Cell-type selectivity, safety, and manufacture of complex systems. |

8.1 Diagnostic and therapeutic prospects of pH differences between noncancerous and cancerous tissues

Measured pH differences in human tissues provide a quantitative basis for investigating tumor metabolism. Table 10 compares each cancer with noncancerous tissue from the same study and distinguishes in vivo measurements from isolated human specimens. This comparative synthesis has a broader scope than the exogenous CEST MRI systematic module in Section 7.1.

Table 10. pH values in noncancerous and cancerous human tissues

| Organ and tumor Compartment | Noncancerous tissue pH | Cancerous tissue pH | ΔpH | Method and source |
|---|---|---|---|---|
| Brain · glioblastoma $pH_i$ | 7.04 ± 0.01; healthy volunteers (n = 36) | 7.12 ± 0.02; glioblastoma (n = 16) | +0.08 | In vivo $^{31}$P MRS [167] |
| Brain · newly diagnosed glioma $pH_i$ | 7.006 ± 0.012; normal-appearing white matter | 7.057 ± 0.024; whole tumor | +0.051 | In vivo 7 T $^{31}$P MRSI, 12 patients [10] |
| Brain · glioma $pH_e$ estimate | 7.34 ± 0.05; contralateral white matter | 7.44 ± 0.01; tumor region | +0.10 | In vivo 7 T $^{31}$P MRSI, 3 patients [168] |

| Organ and tumor Compartment | Noncancerous tissue pH | Cancerous tissue pH | ΔpH | Method and source |
|---|---|---|---|---|
| Liver · hepatocellular carcinoma $pH_e$ | 7.31 ± 0.12; adjacent parenchyma | 6.66 ± 0.19; carcinoma | −0.65 | In vivo 3 T ioversol CEST MRI, 15 patients [7] |
| Lung · bronchial tumor $pH_e$ | 7.30 ± 0.33; noncancerous tissue (n = 10) | 6.46 ± 0.35; tumor tissue (n = 8) | −0.84 | Ex vivo perfused human lung [169] |
| Breast · primary carcinoma $pH_i$ | ≈7.3; noncancerous organoids | ≈7.5; tumor organoids | ≈+0.2 | Ex vivo fluorescence microscopy, source Figure 1F [170] |
| Colon · adenocarcinoma $pH_i$ | ≈7.2; noncancerous epithelial crypts | ≈7.6; adenocarcinoma crypts | ≈+0.4 | Ex vivo fluorescence microscopy, source Figure 1b [171] |

Note. ΔpH is the difference between the reported tumor and noncancerous tissue means. Values marked ≈ were approximately read from graphs under $CO_2/HCO_3^-$ conditions. The sources' ± conventions are retained. Liver parenchymal pH of 7.31 exceeds the reported phantom calibration range of 6.0–7.2 [7]. Blood phosphate signal may have contributed to the glioma $pH_e$ estimate [168].

Using pH differences in cancer diagnosis

The observed liver tumor–adjacent parenchyma $pH_e$ difference of 0.65 units supports investigation of metabolic maps alongside anatomical MRI [7]. Such maps may help compare acidity in structurally similar lesions. Comparing pH-enhanced and standard MRI against an independent diagnosis in the same patients would quantify the additional diagnostic contribution.

Glioma $pH_i$ mapping offers a way to identify metabolically distinct intratumoral regions. Paech and colleagues reported a positive association with the Ki-67 proliferation index [10], which could be investigated for biopsy targeting and longitudinal surveillance. Ex vivo lung $pH_e$ contrast provides a basis for developing clinical probes. Intracellular changes in breast and colon specimens also open a route to functional characterization of excised tissues [169, 170, 171].

Local pH correction and treatment monitoring

Local elevation of $pH_e$ in acidic tumors is being studied to create conditions more favorable to immune cells. In a pancreatic cancer mouse model, tumor-directed L-DOS47 increased $pH_e$ by an average of 0.13 units, and its combination with anti-PD-1 inhibited growth more than anti-PD-1 alone [144]. Mouse buffering studies also support testing local reduction of acidosis as an adjunct to immunotherapy [146].

Elevated $pH_i$ in breast and colon carcinomas encourages investigation of acid-extrusion systems as treatment targets. Experiments in freshly isolated tissues highlighted $Na^+/HCO_3^-$ cotransport in breast carcinoma and $Na^+/H^+$ exchange in colon adenocarcinoma [170, 171]. Tumor acidity can also activate pH-responsive carriers, provided their release range matches the pH of the compartment they reach [12, 142, 143].

Repeated pH mapping before and after treatment can detect early microenvironmental effects. The animal dichloroacetate study captured time-dependent metabolic responses [21]. Future clinical studies could use baseline maps for stratification and repeated maps to assess target engagement. Linking these changes with tumor response and patient-important outcomes would connect diagnosis with treatment monitoring.

9 Quantitative clinical synthesis of acid–base interventions

UBI, BiCARB, and VALOR-CKD examined different interventions and outcomes in chronic kidney disease [23, 24, 156]. UBI used an open-label comparison with standard care; BiCARB enrolled older patients and prioritized physical function; VALOR-CKD tested a different drug and achieved only a small bicarbonate separation. The corrected UBI doses for years 1–3 were 0.56, 0.55, and 0.54 mmol/kg/day

(correction DOI: 10.1007/s40620-020-00742-z). These trials do not support one undifferentiated judgment about alkalinization.

The 457 and 400 adverse events in BiCARB are event counts, not patient counts [24]. In the cognition pilot, within-group p = 0.03 must be considered alongside the placebo comparison of p = 0.39 [157]. Increased urine pH without altered urinary TGF-β [158], and increased $HCO_3^-$ in a veverimer meta-analysis [159], illustrate why biomarker improvement should not automatically be equated with organ protection.

BICARICU-2 analyzed 627 of 640 randomized patients; 90-day mortality was 62.1% with bicarbonate and 61.7% with control [160]. Reduced RRT initiation does not substitute for lower mortality. The IPD meta-analysis of both BICAR trials included 1016 patients and reported mortality RR 0.96 (95% CI 0.86–1.07) and RRT initiation RR 0.69 (95% CI 0.60–0.79) [22]. Because acidemia is itself an RRT criterion, correcting pH may reduce initiation on that indication without demonstrating renal parenchymal recovery or reduced need across all indications.

In the severe-acidemia subgroup of the IPD meta-analysis, mortality RR was 0.80 (95% CI 0.68–0.93), with interaction p = 0.006 [22]. The abstract and methods used pH ≤7.10, while the results used pH <7.10, leaving classification at exactly 7.10 unclear. Clarification requires the authors' data or analysis code. Although prespecified, the subgroup analysis was interpreted as exploratory and was not adjusted for multiple comparisons. It supports further testing without replacing the overall mortality result.

Table 11. Clinical outcomes of acid–base interventions

| Study and analysis sample | Published quantitative result | Important comparison issue |
|---|---|---|
| UBI, 2019; 740 analyzed [156] | Creatinine doubling: bicarbonate 6.6%, standard care 17.0%; p < 0.001 | Open-label; 795 initial participants differ from 740 analyzed. |
| BiCARB, 2020; 300 randomized [24] | Adjusted SPPB difference −0.4; 95% CI −0.9–0.1; p = 0.15; primary outcome available in 187 | Age ≥60; physical-function endpoint. Missingness and dose differ from UBI. |
| VALOR-CKD, 2024; n = 1480 [23] | Primary renal outcome HR 0.99; 95% CI 0.8–1.2; p = 0.90 | Veverimer; $HCO_3^-$ separation ≈1 mEq/L. Not a direct bicarbonate comparison. |
| Citrate–bicarbonate RCT, 2024; n = 124 [161] | eGFR difference −0.99 mL/min/1.73 m²; 95% CI −2.51–0.93; p = 0.20. Discontinuation 4.8% vs 17.7%; p = 0.02 | Active-drug comparison does not assess benefit versus no treatment. |
| BICAR-ICU, 2018; n = 389 [162] | Primary composite difference −5.5 percentage points; 95% CI −15.2–4.2; p = 0.24 | Overall neutral result; AKI subgroup signal assessed separately from the later trial. |
| BICARICU-2, 2025; 627 analyzed [160] | 90-day mortality difference +0.4 percentage points; 95% CI −7.2–8.0; p = 0.91. RRT difference −15.5 points; 95% CI −23.1–−7.8 | Mortality and RRT are distinct endpoints. |
| BICAR IPD, 2026; n = 1016 [22] | Mortality RR 0.96 (0.86–1.07), p = 0.51; RRT RR 0.69 (0.60–0.79) | Reanalysis of participants from [160] and [162], not a third independent trial. |

Note. CI, confidence interval; HR, hazard ratio; RR, relative risk; RRT, renal replacement therapy; SPPB, Short Physical Performance Battery. Percentage points describe absolute differences between proportions. Estimates were taken from the sources; no new pooled effect or meta-analysis was calculated. Absence of statistical significance was not interpreted as proof of no effect or equivalence.

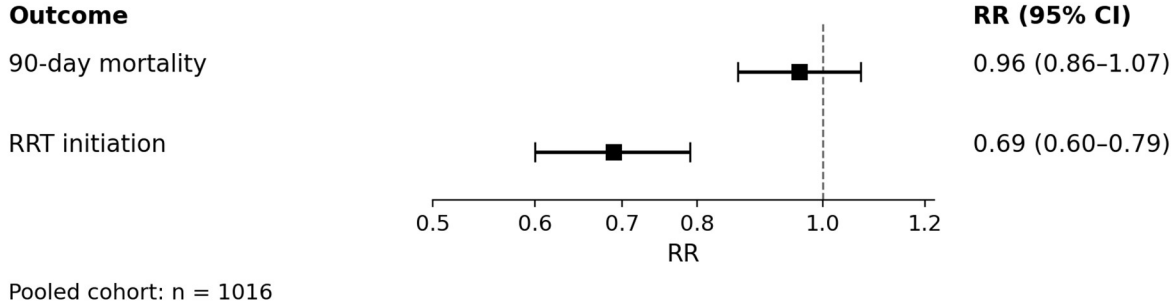



Figure 2. Relative risks and 95% confidence intervals for 90-day mortality and RRT initiation in the published IPD meta-analysis of the two BICAR trials [22]. Estimates and intervals were taken from the source; no new meta-analysis was performed. Both outcomes concern the same pooled cohort. Reduced RRT initiation does not imply reduced mortality.

10 Synthesis of discrepancies and methodological limitations

Differences between findings do not always indicate biological conflict. Apparent discrepancies can arise from mixing $pH_i$, $pH_e$, and luminal pH, measuring different quantities, differing time points or exposure durations, and comparing biochemical with clinical outcomes. Only after these factors have been considered should remaining differences be interpreted as uncertainty about biology or treatment effects [11, 19, 22, 33, 105, 163].

Table 12. Apparent discrepancies, methodological limitations, and ways to resolve them

| Apparent discrepancy | Possible explanation and evidence status | Decisive evaluation |
|---|---|---|
| Higher glioma $pH_i$; lower $pH_e$ in many tumors [7, 10] | Different compartments can coexist biologically. | Coordinated $pH_i$ and $pH_e$ measurements in the same patient. |
| After MPC inhibition, CEST $pH_e$ −0.22; no significant $^{31}P$ NMR change [163] | Compartment, resolution, or sensitivity differences; cause unresolved. | Spatial matching, agent delivery, and a same-compartment reference. |
| Cystic fibrosis acidosis in some studies, no difference in others [98, 99, 100, 104] | Species, age, site, oscillations, and compensation; no single established explanation. | Standard $CO_2$/humidity, calibration, location, and respiratory-cycle protocol. |
| Esomeprazole benefits 4T1, worsens B16-F10 [147] | Tumor and immune context; no universal benefit. | Matched dose, pH target effects, and immune profiling across models. |
| Syrosingopine active in vitro; neutral in vivo $pH_e$ and tumor outcome [135] | Exposure, compensation, or microenvironment remain possible, unseparated causes. | Joint pharmacokinetic, intratumoral drug, and transport-flux assessment. |
| High early ONM-100 findings and poor lung phase II performance [15, 18] | Tumor type, margin versus lesion endpoint, camera, and signal thresholds differ. | Prespecified patient-level criteria and independent histology. |
| UBI favorable; BiCARB and VALOR neutral [23, 24, 156] | Populations, agents, achieved separation, blinding, and endpoints differ. | Multicenter trial with adequate biomarker separation and clinical endpoints. |
| Bicarbonate reduces RRT but not overall mortality [22, 160] | Different endpoints; RRT decisions can depend on pH. | Standardized RRT criteria, renal recovery, and patient-important outcomes. |

| Apparent discrepancy | Possible explanation and evidence status | Decisive evaluation |
|---|---|---|
| Glioma 2025 analysis versus 2024 mapping [10, 88] | 11-patient reanalysis reused earlier data, not an independent cohort. | Trace participant identifiers and recruitment dates. |
| Low DeepCEST RMSE but moderate correlation [8] | Narrow range and possible regression toward the mean. | Independent high-resolution reference and range-specific error/agreement. |

The hemangioma group's mean estimate outside the liver CEST calibration range increases extrapolation uncertainty [7]. Extensive censoring and repeated measurements in the diabetic foot ulcer study also affect the credibility of its thresholds [116]. These limitations should be assessed alongside the main findings.

Cohort overlap was confirmed for ONM-100/HNSCC [18, 136], and the BICAR IPD analysis clearly reused the two parent trials [22, 160, 162]. Publicly available evidence did not permit complete patient-level matching of the initial and subsequent lung reports [15, 16]. They were therefore neither added as independent confirmations nor declared to be entirely identical cohorts.

11 Research implications and future directions

pH is best developed as a functional biomarker defined by compartment, time, and method. Human glioma, liver tumor, wound, and reflux studies illustrate different clinical applications [7, 10, 71, 116]. Tumor acidosis has a strong biological rationale, while diagnostic or therapeutic utility requires both measurement validation and evidence of improved patient outcomes [1, 13, 14, 15, 16, 17, 18].

The following hypotheses arise from the synthesis and remain to be tested.

The $pH_i/pH_e$ gradient and fraction of acidic tumor regions may predict treatment response better than mean pH. Prospective studies should map both compartments alongside perfusion and necrosis and evaluate incremental prognostic value.

In cystic fibrosis, pH oscillation amplitude during a standardized respiratory cycle may better reflect defense function than a static mean. Nasal and bronchial measurements require separate validation.

The efficacy of pH-directed immunotherapy may depend on proton-transport profiles, immune composition, and baseline gradients as well as tumor type. A consistent regimen should be tested across models and then in biomarker-stratified clinical trials.

Machine-learning map errors may differ between low- and high-pH regions. External test sets should be separated by patient and center, with prespecified calibration, Bland–Altman agreement, range-specific errors, and failed-voxel proportions.

Local pH interventions should be evaluated through tumor control, RRT-free days, physical function, or survival in addition to biomarker shifts. Primary outcomes and minimum clinically important differences should be specified before enrollment.

Practical standardization requires consistent recording of compartment, sensor location, calibration range, temperature, $CO_2$ conditions, $B_0/B_1$ correction, contrast dose, low-signal measurements, spatial resolution, and timing. Statistical reports should distinguish patients, animals, cells, sections, and voxels and account for repeated measurements within an individual. This would support fair comparisons between technologies.

12 Conclusion

Meaningful pH assessment begins with a defined biological compartment. Blood, urine, luminal fluid, cytosolic, and organellar pH do not fully represent one another. Electrochemical and optical sensors extend temporal monitoring, while MR methods provide spatial information from deeper tissues. Laboratory resolution, pH sensitivity, and absolute accuracy in patients remain distinct properties [4, 5, 7, 8, 25, 38].

pH changes provide useful information in renal disease, ischemia, airway dysfunction, fibrosis, reflux, and wound healing. Absence of a measured pH difference does not exclude other metabolic abnormalities [38, 86, 99, 100]. Likewise, an intervention-related rise in pH or bicarbonate does not automatically establish improved survival or function [22, 23, 24, 157, 160].

Tumor acidosis is associated with metabolic adaptation, immune function, lipid uptake, and drug resistance. This biology supports diagnostic development, although small pilots and technical feasibility do not establish independent clinical utility [11, 15, 18, 123, 124, 125]. pH-responsive carriers, transport inhibitors, and local buffering each require their own pharmacodynamic and safety evaluation [12, 13, 14, 31, 126].

The bounded systematic analysis of exogenous CEST MRI demonstrated clinical feasibility and promising group differences in human tumor $pH_e$. The selected evidence was insufficient to define a reliable individual-patient threshold. Development should therefore prioritize calibrated, externally validated functional information added to standard MRI [7, 32].

**References**

F — tegishli to‘liq matn bo‘limlari; C — annotatsiya va tanlangan parchalar; A — annotatsiya; A/P — annotatsiya va mavjud preprint. Belgilar sifatni emas, manbadan foydalanish darajasini ko‘rsatadi. Asosiy [1–163] manbalar raqami saqlandi; metodologik [164–166] va qo‘shimcha to‘qima qiyoslari [167–171] kiritildi. Bibliografik yozuvlar nashr tilida, matndagi havolalar raqamli shaklda berildi. Tuzatishlar mustaqil tadqiqot deb sanalmaydi.

F — проверены соответствующие полнотекстовые разделы; C — аннотация и отдельные фрагменты; A — аннотация; A/P — аннотация и доступный препринт. Это уровень доступа, а не качество. Нумерация основных источников [1–163] сохранена; добавлены методические работы [164–166] и тканевые сравнения [167–171]. Библиографические записи сохранены на языке публикации, ссылки в тексте — числовые. Исправления не считаются независимыми исследованиями.

F indicates relevant full-text sections reviewed; C, abstract plus selected excerpts; A, abstract; and A/P, abstract plus an available preprint. These indicate access rather than quality. Core references [1–163] retain their numbering, with methods sources [164–166] and additional tissue comparisons [167–171]. Bibliographic records retain their original publication language; in-text citations are numerical. Corrections are not counted as independent studies.

[1] Swietach, P., Vaughan-Jones, R. D., Harris, A. L., & Hulikova, A. (2014). The chemistry, physiology and pathology of pH in cancer. Philosophical Transactions of the Royal Society B: Biological Sciences, 369(1638), 20130099. https://doi.org/10.1098/rstb.2013.0099 (A)

[2] Damaghi, M., Wojtkowiak, J. W., & Gillies, R. J. (2013). pH sensing and regulation in cancer. Frontiers in Physiology, 4, 370. https://doi.org/10.3389/fphys.2013.00370 (F)

[3] Counillon, L., Bouret, Y., Marchiq, I., & Pouysségur, J. (2016). $Na^+/H^+$ antiporter (NHE1) and lactate/$H^+$ symporters (MCTs) in pH homeostasis and cancer metabolism. Biochimica et Biophysica Acta (BBA) - Molecular Cell Research, 1863(10), 2465-2480. https://doi.org/10.1016/j.bbamcr.2016.02.018 (A)

[4] Corsi, M., Paghi, A., Mariani, S., Golinelli, G., Debrassi, A., Egri, G., Leo, G., Vandini, E., Vilella, A., Dähne, L., Giuliani, D., & Barillaro, G. (2022). Bioresorbable Nanostructured Chemical Sensor for Monitoring of pH Level In Vivo. Advanced Science, 9(22), 2202062. https://doi.org/10.1002/advs.202202062 (F)

[5] Wencel, D., Kaworek, A., Abel, T., Efremov, V., Bradford, A., Carthy, D., Coady, G., McMorrow, R. C. N., & McDonagh, C. (2018). Optical Sensor for Real-Time pH Monitoring in Human Tissue. Small, 14(51), 1803627. https://doi.org/10.1002/smll.201803627 (A)

[6] Madsen, K. E., Hintermueller, D., Opel, E. A., Ribaudo, J. G., Saffari, S., Cho, S., Ciatti, J. L., Huang, Y.-T., Westman, A. M., Nuzzo, R. G., Pet, M. A., & Rogers, J. A. (2026). A miniaturized implantable electrochemical platform for continuous monitoring of metabolites in deep tissue. Science Advances, 12(22), eadz8930. https://doi.org/10.1126/sciadv.adz8930 (F)

[7] Tang, Y., Xiao, G., Shen, Z., Zhuang, C., Xie, Y., Zhang, X., Yang, Z., Guan, J., Shen, Y., Chen, Y., Lai, L., Chen, Y., Chen, S., Dai, Z., Wang, R., & Wu, R. (2020). Noninvasive Detection of Extracellular pH in Human Benign and Malignant Liver Tumors Using CEST MRI. Frontiers in Oncology, 10, 578985. https://doi.org/10.3389/fonc.2020.578985 (F)

[8] Schüre, J.-R., Rajput, J., Shrestha, M., Deichmann, R., Hattingen, E., Maier, A., Nagel, A. M., Dörfler, A., Steidl, E., & Zaiss, M. (2025). Toward Noninvasive High-Resolution In Vivo pH Mapping in Brain Tumors by $^{31}$P-Informed deepCEST MRI. NMR in Biomedicine, 38(6), e70060. https://doi.org/10.1002/nbm.70060 (F)

[9] Grashei, M., Wodtke, P., Skinner, J. G., Sühnel, S., Setzer, N., Metzler, T., Gulde, S., Park, M., Witt, D., Mohr, H., Hundshammer, C., Strittmatter, N., Pellegata, N. S., Steiger, K., & Schilling, F. (2023). Simultaneous magnetic resonance imaging of pH, perfusion and renal filtration using hyperpolarized $^{13}$C-labelled Z-OMPD. Nature Communications, 14(1), 5060. https://doi.org/10.1038/s41467-023-40747-3 (F)

[10] Paech, D., Weckesser, N., Franke, V. L., Breitling, J., Görke, S., Deike-Hofmann, K., Wick, A., Scherer, M., Unterberg, A., Wick, W., Bendszus, M., Bachert, P., Ladd, M. E., Schlemmer, H.-P., & Korzowski, A. (2024). Whole-Brain Intracellular pH Mapping of Gliomas Using High-Resolution $^{31}$P MR Spectroscopic Imaging at 7.0 T. Radiology: Imaging Cancer, 6(1), e220127. https://doi.org/10.1148/rycan.220127 (A)

[11] Li, J., Zhou, Y., Li, X., Yin, S., Gao, Y., Shang, H., Lai, Y., Yang, L., Xue, Y., Li, X., Li, Y., Chang, Z., Chen, J., Cheng, X., Zhang, X., Chu, Q., Lu, F., & Wang, W. (2026). TMEM87A suppresses ferroptosis and increases cancer immunotherapy resistance by maintaining the Golgi apparatus pH homeostasis. Nature Cancer, 7(5), 823-839. https://doi.org/10.1038/s43018-026-01156-9 (F)

[12] Liang, H., Li, G., Zhang, W., Wang, W., Li, D., Cheng, Y., Song, M., Xu, X., & Lu, H. (2026). pH-Responsive Erdafitinib Liposomes with FGFR3 Targeting for Intravesical Bladder Cancer Therapy. International Journal of Molecular Sciences, 27(20), 9014. https://doi.org/10.3390/ijms27209014 (F)

[13] Halford, S., Veal, G. J., Wedge, S. R., Payne, G. S., Bacon, C. M., Sloan, P., Dragoni, I., Heinzmann, K., Potter, S., Salisbury, B. M., Chénard-Poirier, M., Greystoke, A., Howell, E. C., Innes, W. A., Morris, K., Plummer, C., Rata, M., Petrides, G., Keun, H. C., … Plummer, R. (2023). A Phase I Dose-escalation Study of AZD3965, an Oral Monocarboxylate Transporter 1 Inhibitor, in Patients with Advanced Cancer. Clinical Cancer Research, 29(8), 1429-1439. https://doi.org/10.1158/1078-0432.ccr-22-2263 (C)

[14] McDonald, P. C., Chia, S., Bedard, P. L., Chu, Q., Lyle, M., Tang, L., Singh, M., Zhang, Z., Supuran, C. T., Renouf, D. J., & Dedhar, S. (2020). A Phase 1 Study of SLC-0111, a Novel Inhibitor of Carbonic Anhydrase IX, in Patients With Advanced Solid Tumors. American Journal of Clinical Oncology, 43(7), 484-490. https://doi.org/10.1097/coc.0000000000000691 (F)

[15] Kennedy, G. T., Azari, F. S., Chang, A., Bou-Samra, P., Desphande, C., Predina, J., Delikatny, E. J., Olson, M., Rice, D. C., & Singhal, S. (2024). A Phase 2 Multicenter Clinical Trial of Intraoperative Molecular Imaging of Lung Cancer with a pH-Activatable Nanoprobe. Molecular Imaging and Biology, 26(4), 585-592. https://doi.org/10.1007/s11307-024-01933-x (C)

[16] Kennedy, G. T., Azari, F. S., Chang, A., Chang, A., Bou-Samra, P., Desphande, C., Delikatny, E. J., Eruslanov, E., Kucharczuk, J. C., Rice, D. C., & Singhal, S. (2023). A pH-Activatable Nanoprobe Labels Diverse Histologic Subtypes of Human Lung Cancer During Resection. Molecular Imaging and Biology, 25(5), 824-832. https://doi.org/10.1007/s11307-023-01853-2 (C)

[17] Wagner, P., Levine, E. A., Kim, A. C., Shen, P., Fleming, N. D., Westin, S. N., Berry, L. K., Karakousis, G. C., Tanyi, J. L., Olson, M. T., Madajewski, B., Ostrander, B., Krishnan, K., Balch, C. M., & Bartlett, D. L. (2024). Detection of Residual Peritoneal Metastases Following Cytoreductive Surgery Using Pegsitacianine, a pH-Sensitive Imaging Agent: Final Results from a Phase II Study. Annals of Surgical Oncology, 31(7), 4726-4734. https://doi.org/10.1245/s10434-024-15165-4 (A)

[18] Voskuil, F. J., Steinkamp, P. J., Zhao, T., van der Vegt, B., Koller, M., Doff, J. J., Jayalakshmi, Y., Hartung, J. P., Gao, J., Sumer, B. D., Witjes, M. J. H., van Dam, G. M., & SHINE study group. (2020). Exploiting metabolic acidosis in solid cancers using a tumor-agnostic pH-activatable nanoprobe for fluorescence-guided surgery. Nature Communications, 11(1), 3257. https://doi.org/10.1038/s41467-020-16814-4 (F)

[19] Lindeman, L. R., Randtke, E. A., High, R. A., Jones, K. M., Howison, C. M., & Pagel, M. D. (2018). A comparison of exogenous and endogenous CEST MRI methods for evaluating in vivo pH. Magnetic Resonance in Medicine, 79(5), 2766-2772. https://doi.org/10.1002/mrm.26924 (A)

[20] Luan, X., Henao Romero, N., Campanucci, V. A., Le, Y., Mustofa, J., Tam, J. S., & Ianowski, J. P. (2024). Pulmonary Ionocytes Regulate Airway Surface Liquid pH in Primary Human Bronchial Epithelial Cells. American Journal of Respiratory and Critical Care Medicine, 210(6), 788-800. https://doi.org/10.1164/rccm.202309-1565oc (F)

[21] Anemone, A., Consolino, L., Conti, L., Reineri, F., Cavallo, F., Aime, S., & Longo, D. L. (2017). In vivo evaluation of tumour acidosis for assessing the early metabolic response and onset of resistance to dichloroacetate by using magnetic resonance pH imaging. International Journal of Oncology, 51(2), 498-506. https://doi.org/10.3892/ijo.2017.4029 (F)

[22] Fosset, M., Pensier, J., Jabaudon, M., Bitker, L., De Jong, A., Chanques, G., Huguet, H., Molinari, N., Jaber, S., & Jung, B. (2026). Sodium bicarbonate therapy in severe metabolic acidemia: an individual patient data meta-analysis of the BICAR-ICU and BICAR-ICU2 trials. Critical Care, 30(1), 382. https://doi.org/10.1186/s13054-026-06206-3 (F)

[23] Tangri, N., Mathur, V. S., Bushinsky, D. A., Klaerner, G., Li, E., Parsell, D., Stasiv, Y., Walker, M., Wesson, D. E., Wheeler, D. C., Perkovic, V., & Inker, L. A. (2024). VALOR-CKD: A Multicenter, Randomized, Double-Blind Placebo-Controlled Trial Evaluating Veverimer in Slowing Progression of CKD in Patients with Metabolic Acidosis. Journal of the American Society of Nephrology, 35(3), 311-320. https://doi.org/10.1681/asn.0000000000000292 (F)

[24] BiCARB study group. (2020). Clinical and cost-effectiveness of oral sodium bicarbonate therapy for older patients with chronic kidney disease and low-grade acidosis (BiCARB): a pragmatic randomised, double-blind, placebo-controlled trial. BMC Medicine, 18(1), 91. https://doi.org/10.1186/s12916-020-01542-9 (F)

[25] Wu, Y., Zhou, I. Y., Igarashi, T., Longo, D. L., Aime, S., & Sun, P. Z. (2018). A generalized ratiometric chemical exchange saturation transfer (CEST) MRI approach for mapping renal pH using iopamidol. Magnetic Resonance in Medicine, 79(3), 1553-1558. https://doi.org/10.1002/mrm.26817 (A)

[26] Kim, G.-H., & Han, J. S. (2025). Urine pH and Urine Ammonium as Biomarkers in Kidney Disease. Kidney and Blood Pressure Research, 50(1), 644-655. https://doi.org/10.1159/000547775 (A)

[27] Jalihal, U., Mahapatra, J. R., Kumar, A., Bharadwaj, T., Singh, H. D., Mehta, V., Patil, D. R., & Swami, O. C. (2024). Comparative Efficacy of Dexlansoprazole, Pantoprazole, Esomeprazole, and Rabeprazole in Achieving Optimal 24-Hour Intragastric pH Control: A Randomized Crossover Study Using Ambulatory pH Monitoring. Cureus, 16(10), e71418. https://doi.org/10.7759/cureus.71418 (F)

[28] Jacobs, A. I., Prete, M. C., Lesch, A., Sebio, A. A., Teixeira Tarley, C. R., & Swain, G. M. (2024). Measurement of Human and Bovine Exhaled Breath Condensate pH Using Polyaniline-Modified Flexible Inkjet-Printed Nanocarbon Electrodes. ACS Omega, 9(39), 40841-40856. https://doi.org/10.1021/acsomega.4c05800 (F)

[29] Chen, C., Zhang, F., Shen, J., Zheng, Q., Zhang, Z., Lu, S., Liu, L., Zhu, T., Du, Y., & Guan, Y. (2025). CLC3 regulates V-ATPase to enhance lysosomal degradation and cisplatin resistance in cervical cancer cells. Cell Death Discovery, 12(1), 5. https://doi.org/10.1038/s41420-025-02876-0 (F) Tuzatish nashri: https://doi.org/10.1038/s41420-026-03008-y.

[30] Prakash, A., Li, Z., Chirasani, V. R., Rasquinha, J. A., Hewitt, N., Hubbard, G. B., Yin, G., Hawkins, A. T., Montore, L. J., Dohlman, H. G., & Campbell, S. L. (2025). Molecular and functional profiling of Gαi as an intracellular pH sensor. Nature Communications, 16(1), 3468. https://doi.org/10.1038/s41467-025-58323-2 (F)

[31] Qin, H., Tang, D., Li, Z., Yang, F., Wang, J., Liu, X., Chen, C., & Gao, W. (2026). SLC4A7 Drives NSCLC Progression and Immune Evasion via pH Dysregulation: Its Targeting Synergizes with Anti-PD-1/L1 Therapy. International Journal of Biological Sciences, 22(8), 3950-3968. https://doi.org/10.7150/ijbs.129129 (F)

[32] Jones, K. M., Randtke, E. A., Yoshimaru, E. S., Howison, C. M., Chalasani, P., Klein, R. R., Chambers, S. K., Kuo, P. H., & Pagel, M. D. (2017). Clinical Translation of Tumor Acidosis Measurements with

AcidoCEST MRI. Molecular Imaging and Biology, 19(4), 617-625. https://doi.org/10.1007/s11307-016-1029-7 (F)
[33] Stabinska, J., Singh, A., Haney, N. M., Li, Y., Sedaghat, F., Kates, M., & McMahon, M. T. (2023). Noninvasive assessment of renal dynamics and pH in a unilateral ureter obstruction model using DCE MR-CEST urography. Magnetic Resonance in Medicine, 89(1), 343-355. https://doi.org/10.1002/mrm.29436 (A)
[34] Li, Z., Chen, C., & Wang, G. (2026). Negative Pressure Wound Therapy Modulates Wound pH and Bacterial Invasion in Pseudomonas aeruginosa–infected Porcine Wounds. Plastic and Reconstructive Surgery - Global Open, 14(7), e7901. https://doi.org/10.1097/gox.0000000000007901 (F)
[35] Khaled, A., Dhakan, C. B., McCullum, L. B., de la Cerda, J., Schuler, F. W., Li, T., & Pagel, M. D. (2026). A Machine Learning Approach That Measures Extracellular pH Within an In Vivo Tumor Model Using acidoCEST MRI. NMR in Biomedicine, 39(10), e70379. https://doi.org/10.1002/nbm.70379 (F)
[36] Li, T., de La Cerda, J., Tran, R. L., Schuler, F. W., Kotrotsou, A., Zhang, S., Jones, K. M., Trakru, P. N., & Pagel, M. D. (2025). Evaluations of the Bloch fitting method for the analysis of acidoCEST MRI. Magnetic Resonance in Medicine, 94(3), 1218-1226. https://doi.org/10.1002/mrm.30511 (A)
[37] Ali, S. O., Fessas, P., Kaggie, J. D., Zaccagna, F., Houston, G., Reid, S., Graves, M. J., & Gallagher, F. A. (2019). Evaluation of the sensitivity of R1ρ MRI to pH and macromolecular density. Magnetic Resonance Imaging, 58, 156-161. https://doi.org/10.1016/j.MRI.2019.02.004 (F)
[38] Valkovič, L., Clarke, W. T., Schmid, A. I., Raman, B., Ellis, J., Watkins, H., Robson, M. D., Neubauer, S., & Rodgers, C. T. (2019). Measuring inorganic phosphate and intracellular pH in the healthy and hypertrophic cardiomyopathy hearts by in vivo 7T $^{31}$P-cardiovascular magnetic resonance spectroscopy. Journal of Cardiovascular Magnetic Resonance, 21(1), 19. https://doi.org/10.1186/s12968-019-0529-4 (F)
[39] Zhang, X., Gan, H., Shen, Z., Lin, F., Xiao, G., & Wu, R. (2026). Construction of a quantitative extracellular pH map of rat brain glioma using CEST-MRI with iobitridol as the contrast agent. Scientific Reports, 16(1), 21267. https://doi.org/10.1038/s41598-026-51466-2 (F)
[40] Li, T., Cárdenas-Rodríguez, J., Trakru, P. N., & Pagel, M. D. (2023). A machine learning approach that measures pH using acidoCEST MRI of iopamidol. NMR in Biomedicine, 36(10), e4986. https://doi.org/10.1002/nbm.4986 (A)
[41] Romdhane, F., Villano, D., Irrera, P., Consolino, L., & Longo, D. L. (2021). Evaluation of a similarity anisotropic diffusion denoising approach for improving in vivo CEST-MRI tumor pH imaging. Magnetic Resonance in Medicine, 85(6), 3479-3496. https://doi.org/10.1002/mrm.28676 (A)
[42] Kombala, C. J., Kotrotsou, A., Schuler, F. W., de la Cerda, J., Ma, J. C., Zhang, S., & Pagel, M. D. (2021). Development of a Nanoscale Chemical Exchange Saturation Transfer Magnetic Resonance Imaging Contrast Agent That Measures pH. ACS Nano, 15(12), 20678-20688. https://doi.org/10.1021/acsnano.1c10107 (A)
[43] Kombala, C. J., Lokugama, S. D., Kotrotsou, A., Li, T., Pollard, A. C., & Pagel, M. D. (2021). Simultaneous Evaluations of pH and Enzyme Activity with a CEST MRI Contrast Agent. ACS Sensors, 6(12), 4535-4544. https://doi.org/10.1021/acssensors.1c02408 (A)
[44] Goldenberg, J. M., & Pagel, M. D. (2019). Assessments of tumor metabolism with CEST MRI. NMR in Biomedicine, 32(10), e3943. https://doi.org/10.1002/nbm.3943 (A)
[45] Jardim-Perassi, B. V., Irrera, P., Lau, J. Y. C., Budzevich, M., Whelan, C. J., Abrahams, D., Ruiz, E., Ibrahim-Hashim, A., Damgaci Erturk, S., Longo, D. L., Pilon-Thomas, S. A., & Gillies, R. J. (2023). Intraperitoneal Delivery of Iopamidol to Assess Extracellular pH of Orthotopic Pancreatic Tumor Model by CEST-MRI. Contrast Media & Molecular Imaging, 2023, 1-12. https://doi.org/10.1155/2023/1944970 (F)
[46] Randtke, E. A., Granados, J. C., Howison, C. M., Pagel, M. D., & Cárdenas-Rodríguez, J. (2017). Multislice CEST MRI improves the spatial assessment of tumor pH. Magnetic Resonance in Medicine, 78(1), 97-106. https://doi.org/10.1002/mrm.26348 (A)
[47] Shimolina, L., Potekhina, E., Druzhkova, I., Lukina, M., Dudenkova, V., Belousov, V., Shcheslavskiy, V., Zagaynova, E., & Shirmanova, M. (2022). Fluorescence lifetime-based pH mapping of tumors in vivo

using genetically encoded sensor SypHerRed. Biophysical Journal, 121(7), 1156-1165. https://doi.org/10.1016/j.bpj.2022.02.036 (A)
[48] Ong, T. T., Ang, Z., Verma, R., Koean, R., Tam, J. K. C., & Ding, J. L. (2020). pHLuc, a Ratiometric Luminescent Reporter for in vivo Monitoring of Tumor Acidosis. Frontiers in Bioengineering and Biotechnology, 8, 412. https://doi.org/10.3389/fbioe.2020.00412 (F)
[49] Ryan, L. S., Gerberich, J., Haris, U., Nguyen, D., Mason, R. P., & Lippert, A. R. (2020). Ratiometric pH Imaging Using a 1,2-Dioxetane Chemiluminescence Resonance Energy Transfer Sensor in Live Animals. ACS Sensors, 5(9), 2925-2932. https://doi.org/10.1021/acssensors.0c01393 (A)
[50] Zhao, T., Lin, W., Gao, F., Zhao, J., Zhang, J., Di, D., Pei, D., Yang, L., & Hai, J. (2025). Engineering of an Enzyme-Activatable Ratiometric DNA Nanosensor for Spatially Resolved pH Imaging in Ischemic Stroke. Analytical Chemistry, 97(46), 25908-25915. https://doi.org/10.1021/acs.analchem.5c05918 (A)
[51] Zhao, J., Liu, D., Tong, Q., Yuan, J., Hua, Y., Wang, X., Yang, F., & Wu, L. (2026). An Activatable Ratiometric Photoacoustic/Near-Infrared-II Fluorescence Dual-Modal Probe for in vivo Imaging of pH. Analytical Chemistry, 98(29), 21615-21623. https://doi.org/10.1021/acs.analchem.6c02247 (A)
[52] Eubank, T. D., Bobko, A. A., Hoblitzell, E. H., Gencheva, M., Driesschaert, B., & Khramtsov, V. V. (2024). In Vivo Electron Paramagnetic Resonance Molecular Profiling of Tumor Microenvironment upon Tumor Progression to Malignancy in an Animal Model of Breast Cancer. Molecular Imaging and Biology, 26(3), 424-434. https://doi.org/10.1007/s11307-023-01847-0 (A)
[53] Bøgh, N., Hansen, E. S. S., Mariager, C. Ø., Bertelsen, L. B., Ringgaard, S., & Laustsen, C. (2020). Cardiac pH-Imaging With Hyperpolarized MRI. Frontiers in Cardiovascular Medicine, 7, 603674. https://doi.org/10.3389/fcvm.2020.603674 (F)
[54] Lau, A. Z., Miller, J. J., & Tyler, D. J. (2017). Mapping of intracellular pH in the in vivo rodent heart using hyperpolarized [1-$^{13}$C]pyruvate. Magnetic Resonance in Medicine, 77(5), 1810-1817. https://doi.org/10.1002/mrm.26260 (F)
[55] Gallagher, F. A., Kettunen, M. I., Day, S. E., Hu, D.-E., Ardenkjær-Larsen, J. H., in 't Zandt, R., Jensen, P. R., Karlsson, M., Golman, K., Lerche, M. H., & Brindle, K. M. (2008). Magnetic resonance imaging of pH in vivo using hyperpolarized $^{13}$C-labelled bicarbonate. Nature, 453(7197), 940-943. https://doi.org/10.1038/nature07017 (A)
[56] Chen, J., Hackett, E. P., Singh, J., Kovács, Z., & Park, J. M. (2020). Simultaneous Assessment of Intracellular and Extracellular pH Using Hyperpolarized [1- $^{13}$C]Alanine Ethyl Ester. Analytical Chemistry, 92(17), 11681-11686. https://doi.org/10.1021/acs.analchem.0c01568 (A)
[57] Korenchan, D. E., Gordon, J. W., Subramaniam, S., Sriram, R., Baligand, C., VanCriekinge, M., Bok, R., Vigneron, D. B., Wilson, D. M., Larson, P. E. Z., Kurhanewicz, J., & Flavell, R. R. (2019). Using bidirectional chemical exchange for improved hyperpolarized [ $^{13}$C]bicarbonate pH imaging. Magnetic Resonance in Medicine, 82(3), 959-972. https://doi.org/10.1002/mrm.27780 (A)
[58] Mu, C., Liu, X., Kim, Y., Riselli, A., Korenchan, D. E., Bok, R. A., Delos Santos, R., Sriram, R., Qin, H., Nguyen, H., Gordon, J. W., Slater, J., Larson, P. E. Z., Vigneron, D. B., Kurhanewicz, J., Wilson, D. M., & Flavell, R. R. (2023). Clinically Translatable Hyperpolarized $^{13}$C Bicarbonate pH Imaging Method for Use in Prostate Cancer. ACS Sensors, 8(11), 4042-4054. https://doi.org/10.1021/acssensors.3c00851 (F)
[59] Jalal, N. R., Madrakian, T., Ahmadi, M., Afkhami, A., Khalili, S., Bahrami, M., & Roshanaei, M. (2024). Wireless wearable potentiometric sensor for simultaneous determination of pH, sodium and potassium in human sweat. Scientific Reports, 14(1), 11526. https://doi.org/10.1038/s41598-024-62236-3 (F)
[60] Cho, N. S., Hagiwara, A., Yao, J., Nathanson, D. A., Prins, R. M., Wang, C., Raymond, C., Desousa, B. R., Divakaruni, A., Morrow, D. H., Nghiemphu, P. L., Lai, A., Liau, L. M., Everson, R. G., Salamon, N., Pope, W. B., Cloughesy, T. F., & Ellingson, B. M. (2023). Amine-weighted chemical exchange saturation transfer magnetic resonance imaging in brain tumors. NMR in Biomedicine, 36(6), e4785. https://doi.org/10.1002/nbm.4785 (A)

[61] Schüre, J.-R., Shrestha, M., Breuer, S., Deichmann, R., Hattingen, E., Wagner, M., & Pilatus, U. (2019). The pH sensitivity of APT-CEST using phosphorus spectroscopy as a reference method. NMR in Biomedicine, 32(11), e4125. https://doi.org/10.1002/nbm.4125 (A)

[62] Wu, Y., & Sun, P. Z. (2023). Demonstration of pH imaging in acute stroke with endogenous ratiometric chemical exchange saturation transfer magnetic resonance imaging at 2 ppm. NMR in Biomedicine, 36(3), e4850. https://doi.org/10.1002/nbm.4850 (A)

[63] Mu, C., Liu, X., Riselli, A., Slater, J., Escobar, E., Dang, D., Drapeau, S., Delos Santos, R., Andosca, S., Nguyen, H., Larson, P. E. Z., Bok, R., Vigneron, D. B., Kurhanewicz, J., Wilson, D. M., & Flavell, R. R. (2024). Protocol for producing hyperpolarized $^{13}$C-bicarbonate for clinical MRI of extracellular pH in aggressive tumors. STAR Protocols, 5(3), 103091. https://doi.org/10.1016/j.xpro.2024.103091 (F)

[64] Brück, J., Schauenburg, D., Kuan, S. L., Göttert, S., Klasen, B., Frommberger, V., Jalal, K. E., Boui, N., Kwiatkowski, A., Schake, L., Bopp, T., Bohn, T., Weil, T., Schreckenberger, M., & Miederer, M. (2026). Non-invasive visualization of pH changes within the tumor-micro-environment by positron emission tomography. EJNMMI Research, 16(1), 38. https://doi.org/10.1186/s13550-026-01383-2 (F)

[65] Bhatt, G. C., Krishnamurthy, S., Sinha, A., Mittal, A., Kumar, M., Vijay, N., Deepthi, B., Athira, P., Aparna, K. V., Thergaonkar, R., Pakhare, A., Krishnasamy, S., Yadav, M., Mishra, K., Dhingra, B., Singh, K., Kumar, A., Kumar, A., Sharma, T., … Bagga, A. (2026). Clinical and genetic spectrum of distal renal tubular acidosis in children: findings from Indian tubular disorders registry. Pediatric Nephrology. https://doi.org/10.1007/s00467-026-07505-1 (A)

[66] Giaccari, M., Veligratli, F., Hayes, W., Topaloglu, R., Ozdemir, G., Ruggiero, B., Boyer, O., Knebelmann, B., Nedelec, Y., Fila, M., Hemery, F., Atmis, B., Bayazit, A. K., Bertholet-Thomas, A., Lemoine, S., Papizh, S., Prikhodina, L., Aksu, B., La Scola, C., … Emma, F. (2026). The European distal renal tubular acidosis registry: a 5-year analysis. Nephrology Dialysis Transplantation, 41(10), 1839-1848. https://doi.org/10.1093/ndt/gfag051 (A)

[67] Zhou, H., Abdulnour-Nakhoul, S., Hamm, L. L., & Nakhoul, N. L. (2026). Mutations in ammonia transporter RhBG that impair $NH_3/NH_4^+$ transport in patients with chronic kidney disease. The Journal of Physiology, 604(5), 2302-2335. https://doi.org/10.1113/jp288958 (F)

[68] Irrera, P., Consolino, L., Cutrin, J. C., Zöllner, F. G., & Longo, D. L. (2020). Dual assessment of kidney perfusion and pH by exploiting a dynamic CEST-MRI approach in an acute kidney ischemia–reperfusion injury murine model. NMR in Biomedicine, 33(6), e4287. https://doi.org/10.1002/nbm.4287 (A)

[69] Longo, D. L., Cutrin, J. C., Michelotti, F., Irrera, P., & Aime, S. (2017). Noninvasive evaluation of renal pH homeostasis after ischemia reperfusion injury by CEST-MRI. NMR in Biomedicine, 30(7), e3720. https://doi.org/10.1002/nbm.3720 (A)

[70] Chan, J. Y. M., Tan, Y. J., Islahudin, F., & Tan, C. H. H. (2026). Longitudinal impact of sodium bicarbonate therapy on health-related quality of life in pre-dialysis chronic kidney disease with metabolic acidosis: a pragmatic trial in Malaysia. Quality of Life Research, 35(10), 297. https://doi.org/10.1007/s11136-026-04404-8 (A)

[71] Gyawali, C. P., Yadlapati, R., Fass, R., Katzka, D., Pandolfino, J., Savarino, E., Sifrim, D., Spechler, S., Zerbib, F., Fox, M. R., Bhatia, S., de Bortoli, N., Cho, Y. K., Cisternas, D., Chen, C.-L., Cock, C., Hani, A., Remes Troche, J. M., Xiao, Y., … Roman, S. (2024). Updates to the modern diagnosis of GERD: Lyon consensus 2.0. Gut, 73(2), 361-371. https://doi.org/10.1136/gutjnl-2023-330616 (F)

[72] Nguyen-Ngo, K., Jafri, K., Majmudar, V. H., Bipat, R., Sykes, W., Pandolfino, J. E., & Tadros, M. (2026). False Positives in Esophageal pH Monitoring: The Pitfalls of Single-Value Interpretation. Diagnostics, 16(20), 3306. https://doi.org/10.3390/diagnostics16203306 (F)

[73] Hashimoto, H., Piskorz, M. M., Olmos, J. I., Arguero, J., Wonaga, A., Guzman, M., Ballerga, E. G., & Olmos, J. A. (2025). Prolonged wireless pH monitoring increases diagnostic yield in patients with reflux symptoms and borderline 24-hour impedance pH. Diseases of the Esophagus, 38(2), doaf030. https://doi.org/10.1093/dote/doaf030 (A)

[74] Litvak, L., Nordgren, R., Lois, A., & Vigneswaran, Y. (2026). Fixed-distance pH probe placement produces systematic bias in reflux detection: the role of esophageal length. Journal of Gastrointestinal Surgery, 30(11), 102578. https://doi.org/10.1016/j.gassur.2026.102578 (A)
[75] Rusu, R. I., Fox, M. R., Sweis, R., Zeki, S., Dunn, J. M., Anggiansah, A., Jafari, J., Learoyd, A., & Wong, T. (2026). The Optimal Duration of pH Monitoring: Testing the Validity of Lyon 2.0 Recommendations for Wireless pH Measurement. Clinical Gastroenterology and Hepatology, 24(2), 365-374.e7. https://doi.org/10.1016/j.cgh.2024.11.009 (A)
[76] Latorre-Rodríguez, A. R., Pidathala, S., Bremner, R. M., & Mittal, S. K. (2025). pHoenix Score: Validation of a Novel Metric to Improve Diagnosis of Gastroesophageal Reflux Disease Using 24-Hour pH Monitoring. Neurogastroenterology & Motility, 37(11), e70147. https://doi.org/10.1111/nmo.70147 (A)
[77] Siboni, S., Mema, J., McCarthy, T., De Maron, R., Schroeder, M. K., Sozzi, M., Riva, C. G., Asti, E., & Prakash Gyawali, C. (2026). Validation of the Milan Score Using Prolonged Wireless PH Monitoring. Alimentary Pharmacology & Therapeutics, 64(2), 177-185. https://doi.org/10.1111/apt.70668 (A)
[78] Geiken, A., Gutman, A. S., Röder, N., Holtmann, L., Graetz, C., Schwarz, K., & Dörfer, C. E. (2025). A new method for continuous in vivo pH measurement in saliva and oral biofilm - a comparative pilot study. Clinical Oral Investigations, 30(1), 23. https://doi.org/10.1007/s00784-025-06703-9 (F)
[79] Matsumura, T., Sonoda, M., Suzuki, T., Hoppo, T., Seki, Y., Ozaki, T., Takahashi, S., Arakawa, H., Iwasaki, M., Ishikawa, T., Kaneko, T., Ohta, Y., Taida, T., Dao, H. V., Kikuchi, A., Okimoto, K., & Kato, J. (2026). Limitations of 24-hour MII-pH monitoring to diagnose functional heartburn: a diagnostic reassessment. Diseases of the Esophagus, 39(2), doag034. https://doi.org/10.1093/dote/doag034 (A)
[80] Patel, D., Mathews, S., van Unen, V., Chan, J. E., Al-Hammadi, N., Borowitz, D., Gelfond, D., & Sellers, Z. M. (2023). Impaired distal colonic pH in adults with cystic fibrosis. Journal of Cystic Fibrosis, 22(2), 290-295. https://doi.org/10.1016/j.jcf.2022.12.011 (F)
[81] Kelmanson, I. V., Shokhina, A. G., Kotova, D. A., Pochechuev, M. S., Ivanova, A. D., Kostyuk, A. I., Panova, A. S., Borodinova, A. A., Solotenkov, M. A., Stepanov, E. A., Raevskii, R. I., Moshchenko, A. A., Pak, V. V., Ermakova, Y. G., van Belle, G. J. C., Tarabykin, V., Balaban, P. M., Fedotov, I. V., Fedotov, A. B., … Bilan, D. S. (2021). In vivo dynamics of acidosis and oxidative stress in the acute phase of an ischemic stroke in a rodent model. Redox Biology, 48, 102178. https://doi.org/10.1016/j.redox.2021.102178 (F)
[82] Li, M.-H., Leng, T.-D., Feng, X.-C., Yang, T., Simon, R. P., & Xiong, Z.-G. (2016). Modulation of Acid-sensing Ion Channel 1a by Intracellular pH and Its Role in Ischemic Stroke. Journal of Biological Chemistry, 291(35), 18370-18383. https://doi.org/10.1074/jbc.m115.713636 (A)
[83] Komilova, N. R., Angelova, P. R., Berezhnov, A. V., Stelmashchuk, O. A., Mirkhodjaev, U. Z., Houlden, H., Gourine, A. V., Esteras, N., & Abramov, A. Y. (2022). Metabolically induced intracellular pH changes activate mitophagy, autophagy, and cell protection in familial forms of Parkinson's disease. The FEBS Journal, 289(3), 699-711. https://doi.org/10.1111/febs.16198 (A)
[84] Momosaka, D., Togao, O., Kikuchi, K., Kikuchi, Y., Wakisaka, Y., & Hiwatashi, A. (2020). Correlations of amide proton transfer-weighted MRI of cerebral infarction with clinico-radiological findings. PLOS ONE, 15(8), e0237358. https://doi.org/10.1371/journal.pone.0237358 (F)
[85] Stovell, M. G., Mada, M. O., Carpenter, T. A., Yan, J.-L., Guilfoyle, M. R., Jalloh, I., Welsh, K. E., Helmy, A., Howe, D. J., Grice, P., Mason, A., Giorgi-Coll, S., Gallagher, C. N., Murphy, M. P., Menon, D. K., Hutchinson, P. J., & Carpenter, K. L. (2020). Phosphorus spectroscopy in acute TBI demonstrates metabolic changes that relate to outcome in the presence of normal structural MRI. Journal of Cerebral Blood Flow & Metabolism, 40(1), 67-84. https://doi.org/10.1177/0271678x18799176 (F) Tuzatish nashri: https://doi.org/10.1177/0271678X19853211.
[86] Zhu, X.-H., Lee, B.-Y., Tuite, P., Coles, L., Sathe, A. G., Chen, C., Cloyd, J., Low, W. C., Steer, C. J., & Chen, W. (2021). Quantitative Assessment of Occipital Metabolic and Energetic Changes in Parkinson's Patients, Using In Vivo $^{31}$P MRS-Based Metabolic Imaging at 7T. Metabolites, 11(3), 145. https://doi.org/10.3390/metabo11030145 (F)

[87] Caldwell, H. G., Carr, J. M. J. R., Minhas, J. S., Swenson, E. R., & Ainslie, P. N. (2021). Acid–base balance and cerebrovascular regulation. The Journal of Physiology, 599(24), 5337-5359. https://doi.org/10.1113/jp281517 (A)

[88] Franke, V. L., Kroh, F., Seng, B., Platek, J., Weckesser, N., Schlemmer, H.-P., Ladd, M. E., Bachert, P., Paech, D., & Korzowski, A. (2025). Exploring the $^{31}$P chemical shift behavior of high-energy phosphates at 7 T in patients with glioma. Frontiers in Neuroscience, 19, 1638322. https://doi.org/10.3389/fnins.2025.1638322 (F)

[89] Inserte, J., Aluja, D., Barba, I., Ruiz-Meana, M., Miró, E., Poncelas, M., Vilardosa, Ú., Castellano, J., & Garcia-Dorado, D. (2019). High-fat diet improves tolerance to myocardial ischemia by delaying normalization of intracellular PH at reperfusion. Journal of Molecular and Cellular Cardiology, 133, 164-173. https://doi.org/10.1016/j.yjmcc.2019.06.001 (A)

[90] Ciocci Pardo, A., Díaz, R. G., González Arbeláez, L. F., Pérez, N. G., Swenson, E. R., Mosca, S. M., & Alvarez, B. V. (2018). Benzolamide perpetuates acidic conditions during reperfusion and reduces myocardial ischemia-reperfusion injury. Journal of Applied Physiology, 125(2), 340-352. https://doi.org/10.1152/japplphysiol.00957.2017 (F)

[91] Jiang, K., Su, F., Deng, R., Xu, Y., Qin, A., Yuan, X., Xing, D., Chen, Y., Wang, D., Shen, L., Hwa, J., Hou, L., & Xiang, Y. (2025). Cardiomyocyte-specific NHE1 overexpression confers protection against myocardial infarction during hyperglycemia. Cardiovascular Diabetology, 24(1), 184. https://doi.org/10.1186/s12933-025-02743-3 (F)

[92] Meng, Z., Kovacs, B., Yan, C., Hölscher, C., Zhazykbayeva, S., Jarkas, O., Zou, C., Cyganek, L., Zorio, E., Braza-Boils, A., Pablo Ochoa, J., Rehbehn, N., Fan, X., Lei, X., Liu, R., Tong, S., Liu, F., Xue, Z., Bober, S. L., … El-Battrawy, I. (2026). SLC4A3-related short QT syndrome assessed in human induced pluripotent stem cell-derived cardiomyocytes: mechanisms of ventricular arrhythmia and sudden cardiac death. European Heart Journal, 47(23), 2982-2998. https://doi.org/10.1093/eurheartj/ehag068 (A)

[93] Matthews, J. J., Artioli, G. G., Turner, M. D., & Sale, C. (2019). The Physiological Roles of Carnosine and β-Alanine in Exercising Human Skeletal Muscle. Medicine & Science in Sports & Exercise, 51(10), 2098-2108. https://doi.org/10.1249/mss.0000000000002033 (A)

[94] Orlowski, A., Di Mattia, R. A., & Aiello, E. A. (2025). Intracellular pH Regulation in Ventricular Myocytes: Implications for Cardiac Health and Disease. Circulation Research, 136(12), 1636-1656. https://doi.org/10.1161/circresaha.125.325386 (A)

[95] Kandilci, H. B., Richards, M. A., Fournier, M., Şimşek, G., Chung, Y. J., Lakhal-Littleton, S., & Swietach, P. (2021). Cardiomyocyte $Na^+/H^+$ Exchanger-1 Activity Is Reduced in Hypoxia. Frontiers in Cardiovascular Medicine, 7, 617038. https://doi.org/10.3389/fcvm.2020.617038 (F)

[96] Espejo, M. S., Orlowski, A., Sørensen, T. M., Matchkov, V. V., Aiello, E. A., & Boedtkjer, E. (2025). Loss of $Na^+$, $HCO_3^-$–Cotransporter NBCn1 Inhibits Net Acid Extrusion in the Atria and Causes Hypertension-Associated Cardiac Hypertrophy. Acta Physiologica, 241(8), e70078. https://doi.org/10.1111/apha.70078 (F)

[97] Milliken, A. S., Ciesla, J. H., Nadtochiy, S. M., & Brookes, P. S. (2023). Distinct effects of intracellular vs. extracellular acidic pH on the cardiac metabolome during ischemia and reperfusion. Journal of Molecular and Cellular Cardiology, 174, 101-114. https://doi.org/10.1016/j.yjmcc.2022.11.008 (A/P)

[98] Pezzulo, A. A., Tang, X. X., Hoegger, M. J., Abou Alaiwa, M. H., Ramachandran, S., Moninger, T. O., Karp, P. H., Wohlford-Lenane, C. L., Haagsman, H. P., van Eijk, M., Bánfi, B., Horswill, A. R., Stoltz, D. A., McCray, P. B., Welsh, M. J., & Zabner, J. (2012). Reduced airway surface pH impairs bacterial killing in the porcine cystic fibrosis lung. Nature, 487(7405), 109-113. https://doi.org/10.1038/nature11130 (F)

[99] Schultz, A., Puvvadi, R., Borisov, S. M., Shaw, N. C., Klimant, I., Berry, L. J., Montgomery, S. T., Nguyen, T., Kreda, S. M., Kicic, A., Noble, P. B., Button, B., & Stick, S. M. (2017). Airway surface liquid pH is not acidic in children with cystic fibrosis. Nature Communications, 8(1), 1409. https://doi.org/10.1038/s41467-017-00532-5 (F)

[100] Benedetto, R., Centeio, R., Ousingsawat, J., Schreiber, R., Janda, M., & Kunzelmann, K. (2020). Transport properties in CFTR−/− knockout piglets suggest normal airway surface liquid pH and enhanced amiloride-sensitive $Na^+$ absorption. Pflügers Archiv - European Journal of Physiology, 472(10), 1507-1519. https://doi.org/10.1007/s00424-020-02440-y (F)

[101] Davis, M. D., Smith, L., Zhao, Y., Rahman, R. A., Khalid, F., Chmiel, J., Boyne, K., Daniels, I. A., Gaston, B., & Marozkina, N. (2026). Human Nasal and Bronchial Epithelium in Cystic Fibrosis: Differences in Expression of Airway pH Regulatory Proteins. Pediatric Pulmonology, 61(8), e71784. https://doi.org/10.1002/ppul.71784 (F)

[102] Rehman, T., & Welsh, M. J. (2023). Inflammation as a Regulator of the Airway Surface Liquid pH in Cystic Fibrosis. Cells, 12(8), 1104. https://doi.org/10.3390/cells12081104 (F)

[103] Thornell, I. M., Rehman, T., Pezzulo, A. A., & Welsh, M. J. (2020). Paracellular bicarbonate flux across human cystic fibrosis airway epithelia tempers changes in airway surface liquid pH. The Journal of Physiology, 598(19), 4307-4320. https://doi.org/10.1113/jp280120 (A)

[104] Kim, D., Liao, J., Scales, N. B., Martini, C., Luan, X., Abu-Arish, A., Robert, R., Luo, Y., McKay, G. A., Nguyen, D., Tewfik, M. A., Poirier, C. D., Matouk, E., Ianowski, J. P., Frenkiel, S., & Hanrahan, J. W. (2021). Large pH oscillations promote host defense against human airways infection. Journal of Experimental Medicine, 218(4), e20201831. https://doi.org/10.1084/jem.20201831 (F)

[105] Morrison, C. B., Shaffer, K. M., Araba, K. C., Markovetz, M. R., Wykoff, J. A., Quinney, N. L., Hao, S., Delion, M. F., Flen, A. L., Morton, L. C., Liao, J., Hill, D. B., Drumm, M. L., O'Neal, W. K., Kesimer, M., Gentzsch, M., & Ehre, C. (2022). Treatment of cystic fibrosis airway cells with CFTR modulators reverses aberrant mucus properties via hydration. European Respiratory Journal, 59(2), 2100185. https://doi.org/10.1183/13993003.00185-2021 (A)

[106] Tang, X. X., Ostedgaard, L. S., Hoegger, M. J., Moninger, T. O., Karp, P. H., McMenimen, J. D., Choudhury, B., Varki, A., Stoltz, D. A., & Welsh, M. J. (2016). Acidic pH increases airway surface liquid viscosity in cystic fibrosis. Journal of Clinical Investigation, 126(3), 879-891. https://doi.org/10.1172/jci83922 (F)

[107] Abou Alaiwa, M. H., Launspach, J. L., Grogan, B., Carter, S., Zabner, J., Stoltz, D. A., Singh, P. K., McKone, E. F., & Welsh, M. J. (2018). Ivacaftor-induced sweat chloride reductions correlate with increases in airway surface liquid pH in cystic fibrosis. JCI Insight, 3(15), e121468. https://doi.org/10.1172/jci.insight.121468 (F)

[108] Skinner, W. H., Robinson, N., Hardisty, G. R., Gray, R. D., & Campbell, C. J. (2024). SERS Microsensors for the Study of pH Regulation in Cystic Fibrosis Patient-Derived Airway Cultures. ACS Sensors, 9(5), 2550-2557. https://doi.org/10.1021/acssensors.4c00279 (F)

[109] Delpiano, L., Rodenburg, L. W., Burke, M., Nelson, G., Amatngalim, G. D., Beekman, J. M., & Gray, M. A. (2023). Dynamic regulation of airway surface liquid pH by TMEM16A and SLC26A4 in cystic fibrosis nasal epithelia with rare mutations. Proceedings of the National Academy of Sciences, 120(47), e2307551120. https://doi.org/10.1073/pnas.2307551120 (F)

[110] Rehman, T., Karp, P. H., Thurman, A. L., Mather, S. E., Jain, A., Cooney, A. L., Sinn, P. L., Pezzulo, A. A., Duffey, M. E., & Welsh, M. J. (2022). WNK Inhibition Increases Surface Liquid pH and Host Defense in Cystic Fibrosis Airway Epithelia. American Journal of Respiratory Cell and Molecular Biology, 67(4), 491-502. https://doi.org/10.1165/rcmb.2022-0172oc (F)

[111] Kreißl, S., Hendler, S., Akmatov, M. K., von Meien, M., Range, U., Pessler, F., & Vogelberg, C. (2021). Reduced Exhaled Breath Condensate pH and Severity of Allergic Sensitization Predict School Age Asthma. The Journal of Allergy and Clinical Immunology: In Practice, 9(4), 1570-1577. https://doi.org/10.1016/j.jaip.2020.10.058 (A)

[112] Rama, T. A., Paciência, I., Cavaleiro Rufo, J., Silva, D., Cunha, P., Severo, M., Padrão, P., Moreira, P., Delgado, L., & Moreira, A. (2021). Exhaled breath condensate pH determinants in school-aged children: A population-based study. Pediatric Allergy and Immunology, 32(7), 1474-1481. https://doi.org/10.1111/pai.13564 (A)

[113] Li, J., Yao, S., Zimny, S., Koob, D., Jin, H., Wimmer, R., Denk, G., Tuo, B., & Hohenester, S. (2024). The acidic microenvironment in the perisinusoidal space critically determines bile salt-induced activation of hepatic stellate cells. Communications Biology, 7(1), 1591. https://doi.org/10.1038/s42003-024-07192-4 (F)
[114] Sjøgaard-Frich, L. M., Henriksen, M. S., Lam, S. M., Birkbak, F. J., Czaplinska, D., Flinck, M., & Pedersen, S. F. (2024). NHE1 regulation in NAFLD in vitro contributes to hepatocyte injury and HSC crosstalk. Journal of Endocrinology, 263(2), e240099. https://doi.org/10.1530/joe-24-0099 (A)
[115] Marrone, G., De Chiara, F., Böttcher, K., Levi, A., Dhar, D., Longato, L., Mazza, G., Zhang, Z., Marrali, M., Fernández-Iglesias, A., Hall, A., Luong, T. V., Viollet, B., Pinzani, M., & Rombouts, K. (2018). The adenosine monophosphate–activated protein kinase–vacuolar adenosine triphosphatase–pH axis: A key regulator of the profibrogenic phenotype of human hepatic stellate cells. Hepatology, 68(3), 1140-1153. https://doi.org/10.1002/hep.30029 (A)
[116] Sukarni, S., Jais, S., Haryanto, H., Aminuddin, M., Mukai, K., Okuwa, M., & Oe, M. (2026). Optimal Wound pH and Related Factors in the Healing Process of Diabetes-Related Foot Ulcer: A Prospective Observational Study. Health Science Reports, 9(3), e72079. https://doi.org/10.1002/hsr2.72079 (F)
[117] Li, T., & Tuo, B. (2020). Pathophysiology of hepatic $Na^+/H^+$ exchange (Review). Experimental and Therapeutic Medicine, 20(2), 1220-1229. https://doi.org/10.3892/etm.2020.8888 (F)
[118] Dong, S., Shewarega, A., Chapiro, J., Cai, Z., Hyder, F., Coman, D., & Duncan, J. S. (2024). High-resolution extracellular pH imaging of liver cancer with multiparametric MR using Deep Image Prior. NMR in Biomedicine, 37(8), e5145. https://doi.org/10.1002/nbm.5145 (A)
[119] Ma, Y.-J., High, R. A., Tang, Q., Wan, L., Jerban, S., Du, J., & Chang, E. Y. (2019). AcidoCEST-UTE MRI for the Assessment of Extracellular pH of Joint Tissues at 3 T. Investigative Radiology, 54(9), 565-571. https://doi.org/10.1097/rli.0000000000000576 (A)
[120] Lombardi, A. F., Ma, Y., Jang, H., Jerban, S., Tang, Q., Searleman, A. C., Meyer, R. S., Du, J., & Chang, E. Y. (2022). AcidoCEST-UTE MRI Reveals an Acidic Microenvironment in Knee Osteoarthritis. International Journal of Molecular Sciences, 23(8), 4466. https://doi.org/10.3390/ijms23084466 (F) Tuzatish nashri: https://doi.org/10.3390/ijms241512346.
[121] Sukarni, S., Aminuddin, M., Kunimitsu, M., Mukai, K., Okuwa, M., Haryanto, H., Jais, S., & Oe, M. (2025). Trigona honey effect on wound pH and healing in diabetes-related foot ulcers: A case series. Complementary Therapies in Clinical Practice, 59, 101975. https://doi.org/10.1016/j.ctcp.2025.101975 (A)
[122] Groessl, S., Kalis, R., Snaebjornsson, M. T., Wambach, L., Haider, J., Andersch, F., Schulze, A., Palm, W., & Zuber, J. (2025). Acidosis orchestrates adaptations of energy metabolism in tumors. Science, 390(6769), eadp7603. https://doi.org/10.1126/science.adp7603 (A)
[123] Severin, M., Hansen, R. K., Rolver, M. G., Hels, T., Maeda, K., Pardo, L. A., & Pedersen, S. F. (2025). Tumor acidosis supports cancer cell lipid uptake via a rapid transporter-independent mechanism. Journal of Cell Science, 138(10), jcs263688. https://doi.org/10.1242/jcs.263688 (A)
[124] Bång-Rudenstam, A., Cerezo-Magaña, M., Horvath, M., Talbot, H., Gustafsson, E., Jonathan, S., Chakraborty, C., Nissen, I., Gonçalves de Oliveira, K., Boukredine, A., Beyer, S., Perez, J. E., Johansson, M. C., Kjellén, L., Tykesson, E., Malmström, A., van Kuppevelt, T. H., Forsberg-Nilsson, K., Esko, J. D., … Belting, M. (2026). Tumour acidosis remodels the glycocalyx to control lipid scavenging and ferroptosis. Nature Cell Biology, 28(3), 567-580. https://doi.org/10.1038/s41556-026-01879-y (F)
[125] Harmon, C., Robinson, M. W., Hand, F., Almuaili, D., Mentor, K., Houlihan, D. D., Hoti, E., Lynch, L., Geoghegan, J., & O'Farrelly, C. (2019). Lactate-Mediated Acidification of Tumor Microenvironment Induces Apoptosis of Liver-Resident NK Cells in Colorectal Liver Metastasis. Cancer Immunology Research, 7(2), 335-346. https://doi.org/10.1158/2326-6066.cir-18-0481 (F)
[126] Oluwatola, O., Bazargan, S., Irrera, P., Chang, D., Thomas, A., Blauvelt, J., Beatty, M., Hall, M., Whelan, C. J., Estrella, V., Rejniak, K. A., Poch, M., Fitzsimmons, N., Beal, R., Ibrahim-Hashim, A., & Pilon-Thomas, S. (2026). Transdermal bicarbonate buffer therapy increases intratumoral pH and elicits antitumor responses in bladder cancer. Frontiers in Immunology, 17, 1706250. https://doi.org/10.3389/fimmu.2026.1706250 (F)

[127] Chen, C., Wang, X., Yang, T., Yuan, X., Liang, N., Yang, Y., Yang, X., Pang, Y., Zhao, Y., & Li, C. (2026). The pH perspective of cancer: From warburg's misconception to therapeutic targeting of pH regulating proteins. Critical Reviews in Oncology/Hematology, 217, 105051. https://doi.org/10.1016/j.critrevonc.2025.105051 (A)

[128] Hulikova, A., & Swietach, P. (2026). Using Mathematical Modeling of Tumor Metabolism to Predict the Magnitude, Composition, and Hypoxic Interactions of Microenvironment Acidosis. BioEssays, 48(1), e70101. https://doi.org/10.1002/bies.70101 (F)

[129] Lombardi, A. F., Wong, J. H., High, R., Ma, Y., Jerban, S., Tang, Q., Du, J., Frost, P., Pagel, M. D., & Chang, E. Y. (2021). AcidoCEST MRI Evaluates the Bone Microenvironment in Multiple Myeloma. Molecular Imaging and Biology, 23(6), 865-873. https://doi.org/10.1007/s11307-021-01611-2 (A)

[130] Corrado, A., Lorito, N., Anemone, A., Carella, A., Villano, D., Pirotta, E., Gammaraccio, F., Subbiani, A., Bacci, M., Dastrù, W., Morandi, A., & Longo, D. L. (2025). In vivo imaging of the spatial heterogeneity of intratumoral acidosis (pH) as a marker of the metastatic phenotype in breast cancer. Breast Cancer Research, 27(1), 112. https://doi.org/10.1186/s13058-025-02065-y (F)

[131] Lee, C.-J., Yun, H.-J., Jang, T.-Y., Jeon, S.-E., Cho, Y.-H., Lim, D.-Y., Han, E.-J., Kong, S.-Y., & Nam, J.-S. (2026). The dysadherin/carbonic anhydrase 9 axis shapes an acidic tumor microenvironment to promote colorectal cancer progression. Signal Transduction and Targeted Therapy, 11(1), 19. https://doi.org/10.1038/s41392-025-02543-x (F)

[132] Christiansen, F. B., Novella, E. S., Lindemann, A. V., Cordes, J. F. H., & Pedersen, S. F. (2026). T Cell Dysfunction in the Acidic Tumor Microenvironment. Acta Physiologica, 242(6), e70260. https://doi.org/10.1111/apha.70260 (A)

[133] Rahman, M. A., Yadab, M. K., & Ali, M. M. (2024). Emerging Role of Extracellular pH in Tumor Microenvironment as a Therapeutic Target for Cancer Immunotherapy. Cells, 13(22), 1924. https://doi.org/10.3390/cells13221924 (F)

[134] Chen, F., Cai, X., Zhou, Q., Huang, Z., Wang, J., Kang, R., Tang, D., & Liu, J. (2026). Compartmental pH regulation in cancer and antitumor immunity: therapeutic opportunities and challenges. Apoptosis, 31(8), 197. https://doi.org/10.1007/s10495-026-02408-w (F)

[135] Buyse, C., Joudiou, N., Warscotte, A., Richiardone, E., Mignion, L., Corbet, C., & Gallez, B. (2022). Evaluation of Syrosingopine, an MCT Inhibitor, as Potential Modulator of Tumor Metabolism and Extracellular Acidification. Metabolites, 12(6), 557. https://doi.org/10.3390/metabo12060557 (F)

[136] Steinkamp, P. J., Voskuil, F. J., van der Vegt, B., Doff, J. J., Schepman, K.-P., de Visscher, S. A. H. J., Kelder, W., Jayalakshmi, Y., Gao, J., Sumer, B. D., van Dam, G. M., & Witjes, M. J. H. (2021). A Standardized Framework for Fluorescence-Guided Margin Assessment for Head and Neck Cancer Using a Tumor Acidosis Sensitive Optical Imaging Agent. Molecular Imaging and Biology, 23(6), 809-817. https://doi.org/10.1007/s11307-021-01614-z (F)

[137] Lindeman, L. R., Jones, K. M., High, R. A., Howison, C. M., Shubitz, L. F., & Pagel, M. D. (2019). Differentiating lung cancer and infection based on measurements of extracellular pH with acidoCEST MRI. Scientific Reports, 9(1), 13002. https://doi.org/10.1038/s41598-019-49514-1 (F)

[138] Chen, M., Chen, C., Shen, Z., Zhang, X., Chen, Y., Lin, F., Ma, X., Zhuang, C., Mao, Y., Gan, H., Chen, P., Zong, X., & Wu, R. (2017). Extracellular pH is a biomarker enabling detection of breast cancer and liver cancer using CEST MRI. Oncotarget, 8(28), 45759-45767. https://doi.org/10.18632/oncotarget.17404 (F)

[139] High, R. A., Randtke, E. A., Jones, K. M., Lindeman, L. R., Ma, J. C., Zhang, S., LeRoux, L. G., & Pagel, M. D. (2019). Extracellular acidosis differentiates pancreatitis and pancreatic cancer in mouse models using acidoCEST MRI. Neoplasia, 21(11), 1085-1090. https://doi.org/10.1016/j.neo.2019.09.004 (F)

[140] Longo, D. L., Bartoli, A., Consolino, L., Bardini, P., Arena, F., Schwaiger, M., & Aime, S. (2016). In Vivo Imaging of Tumor Metabolism and Acidosis by Combining PET and MRI-CEST pH Imaging. Cancer Research, 76(22), 6463-6470. https://doi.org/10.1158/0008-5472.can-16-0825 (A)

[141] Korenchan, D. E., Bok, R., Sriram, R., Liu, K., Santos, R. D., Qin, H., Lobach, I., Korn, N., Wilson, D. M., Kurhanewicz, J., & Flavell, R. R. (2019). Hyperpolarized in vivo pH imaging reveals grade-dependent acidification in prostate cancer. Oncotarget, 10(58), 6096-6110. https://doi.org/10.18632/oncotarget.27225 (F)

[142] Tapponi, S., Yusuf, A., Alsaafin, F., & Hussain, Z. (2025). Breaking barriers with pH-responsive nanocarriers: a new frontier in precision oncology. International Journal of Pharmaceutics, 682, 125931. https://doi.org/10.1016/j.ijpharm.2025.125931 (A)

[143] Liu, Y., Si, L., Jiang, Y., Jiang, S., Zhang, X., Li, S., Chen, J., & Hu, J. (2025). Design of pH-Responsive Nanomaterials Based on the Tumor Microenvironment. International Journal of Nanomedicine, Volume 20, 705-721. https://doi.org/10.2147/ijn.s504629 (F)

[144] Jardim-Perassi, B. V., Irrera, P., Oluwatola, O. E., Abrahams, D., Estrella, V. C., Ordway, B., Byrne, S. R., Ojeda, A. A., Whelan, C. J., Kim, J., Beatty, M. S., Damgaci-Erturk, S., Longo, D. L., Gaspar, K. J., Siegers, G. M., Centeno, B. A., Lau, J. Y. C., Pilon-Thomas, S. A., Ibrahim-Hashim, A., & Gillies, R. J. (2024). L-DOS47 Elevates Pancreatic Cancer Tumor pH and Enhances Response to Immunotherapy. Biomedicines, 12(2), 461. https://doi.org/10.3390/biomedicines12020461 (F)

[145] Li, F., Su, K., Riaz, F., Liu, C., Wei, P., Li, X., Zhang, K., Zhao, T., Xu, W., Zhao, X., Lu, W. W., Yang, Q., Zhao, L., Pan, F., & Pan, H. (2026). pH-neutralization strategy to suppress GPCR68 spatiotemporally activates T cells and enhances anti-tumor immunity. Bioactive Materials, 61, 601-621. https://doi.org/10.1016/j.bioactmat.2026.02.039 (A)

[146] Pilon-Thomas, S., Kodumudi, K. N., El-Kenawi, A. E., Russell, S., Weber, A. M., Luddy, K., Damaghi, M., Wojtkowiak, J. W., Mulé, J. J., Ibrahim-Hashim, A., & Gillies, R. J. (2016). Neutralization of Tumor Acidity Improves Antitumor Responses to Immunotherapy. Cancer Research, 76(6), 1381-1390. https://doi.org/10.1158/0008-5472.can-15-1743 (A) Tuzatish nashri: https://doi.org/10.1158/0008-5472.CAN-17-0559.

[147] Tran, R. L., Li, T., de la Cerda, J., Schuler, F. W., Khaled, A. S., Pudakalakatti, S., Bhattacharya, P. K., Sinharay, S., & Pagel, M. D. (2025). Potentiation of immune checkpoint blockade with a pH-sensitizer as monitored in two pre-clinical tumor models with acidoCEST MRI. British Journal of Cancer, 132(8), 744-753. https://doi.org/10.1038/s41416-025-02962-1 (A)

[148] Dhakan, C., Anemone, A., Ventura, V., Carella, A., Corrado, A., Pirotta, E., Villano, D., Romdhane, F., Gammaraccio, F., Aime, S., & Longo, D. L. (2023). Assessing the Therapeutic Efficacy of Proton Transport Inhibitors in a Triple-Negative Breast Cancer Murine Model with Magnetic Resonance Imaging–Chemical Exchange Saturation Transfer Tumor pH Imaging. Metabolites, 13(11), 1161. https://doi.org/10.3390/metabo13111161 (F)

[149] Robey, I. F., Baggett, B. K., Kirkpatrick, N. D., Roe, D. J., Dosescu, J., Sloane, B. F., Hashim, A. I., Morse, D. L., Raghunand, N., Gatenby, R. A., & Gillies, R. J. (2009). Bicarbonate Increases Tumor pH and Inhibits Spontaneous Metastases. Cancer Research, 69(6), 2260-2268. https://doi.org/10.1158/0008-5472.can-07-5575 (A)

[150] Gong, J., Huang, H., Gao, M., Ruan, Y., Chen, R., Li, Y., Wang, S., & Sun, X. (2026). Reshape Intracellular/Extracellular pH for Enhanced Nanocatalytic Ferroptosis and cGAS-STING Activation Induced Immunotherapy. Small, 22(9), e10253. https://doi.org/10.1002/smll.202510253 (A)

[151] Yang, W., Wang, C., Yu, C., Jiang, N., Yu, B., Ni, Y., Ni, C., Feng, L., & Zhang, L. (2026). pH-regulating Lipiodol Pickering emulsions enhance transarterial embolization therapy via inducing ferroptosis and activating antitumor immunity. Cell Reports Medicine, 7(3), 102662. https://doi.org/10.1016/j.xcrm.2026.102662 (F)

[152] Qin, J., He, Y., Yang, Y., Jiao, Y., Liu, Z., Xie, Y., Lu, W., Liu, M., Zhao, Z., Cai, D., & Wang, G. (2026). Spatially programmed Fe and Pt electrode-driven electrochemistry reconditions the tumor microenvironment and sensitizes triple-negative breast cancer to PD-1 Blockade. Frontiers in Oncology, 16, 1819923. https://doi.org/10.3389/fonc.2026.1819923 (F)

[153] Mu, M., Zhang, M., Liu, J., Ren, K., Liu, H., Yip, L., Guo, K., Teng, F., Dong, J., Xu, X., Leong, D. T., & Sun, X. (2025). Real-time magnetic resonance visualization of tumor acidosis as a precognition indicator of therapeutic efficacy. Bioactive Materials, 52, 63-72. https://doi.org/10.1016/j.bioactmat.2025.05.033 (F)

[154] Wang, L., Bai, J., Chen, X., Liu, H., Shi, J., Peng, W., Weng, J., Zhi, W., & Wang, J. (2026). Novel oral pH-responsive dual-targeted nanogels for precision therapy of colorectal cancer. Journal of Materials Chemistry B, 14(7), 2157-2176. https://doi.org/10.1039/d5tb02238j (A)

[155] Jin, G., Yang, Z., Wang, L., Zhang, S., Lin, S., Bi, Z., Yu, B., Su, Y., Xiang, S., Veselova, I. A., Liu, H., Li, F., Wu, S., Li, M., Chen, X., & Lv, S. (2026). pH-responsive polymeric-peptide complex enhances tumor immunogenic cell death by membrane disruption. Journal of Controlled Release, 392, 114660. https://doi.org/10.1016/j.jconrel.2026.114660 (A)

[156] Di Iorio, B. R., Bellasi, A., Raphael, K. L., Santoro, D., Aucella, F., Garofano, L., Ceccarelli, M., Di Lullo, L., Capolongo, G., Di Iorio, M., Guastaferro, P., Capasso, G., & UBI Study Group. (2019). Treatment of metabolic acidosis with sodium bicarbonate delays progression of chronic kidney disease: the UBI Study. Journal of Nephrology, 32(6), 989-1001. https://doi.org/10.1007/s40620-019-00656-5 (F) Tuzatish nashri: https://doi.org/10.1007/s40620-020-00742-z.

[157] Gu, F., You, Z., Hawkins, N., Reddin, R., Hamour, R., Shapiro, A., Coughlan, C., Seals, D., Furgeson, S., Dixon, A., Nowak, K. L., & Kendrick, J. (2025). Effects of sodium bicarbonate therapy on cognitive and cerebrovascular function in midlife and older adults with chronic kidney disease: a pilot randomized trial. BMC Nephrology, 26(1), 454. https://doi.org/10.1186/s12882-025-04388-6 (F)

[158] Ngupis, N., Satirapoj, B., Tangwonglert, T., Supasyndh, O., Thimachai, P., & Siriwattanasit, N. (2025). Effect of oral sodium bicarbonate supplementation on urine TGF-$\boldsymbol{\beta}$ in normal serum bicarbonate CKD, a randomized controlled trial. Scientific Reports, 15(1), 22319. https://doi.org/10.1038/s41598-025-03733-x (F)

[159] Islampanah, M., Karami, S., Salehi, S., Akbari, A., Noradini, A., Tafazolimoghadam, A., Yousefi, S., & Pirzad, S. (2026). Veverimer in treating metabolic acidosis in chronic kidney disease patients: a systematic review and meta-analysis of randomized clinical trials. BMC Nephrology, 27(1), 144. https://doi.org/10.1186/s12882-026-04821-4 (F)

[160] Jung, B., Jabaudon, M., De Jong, A., Bitker, L., Audard, J., Klouche, K., Sarton, B., Guitton, C., Lasocki, S., Rieu, B., Canet, E., Jeantrelle, C., Roquilly, A., Mayaux, J., Verdonk, F., Pottecher, J., Ferrandiere, M., Riu, B., Garcon, P., … BICARICU-2 Study Group. (2025). Sodium Bicarbonate for Severe Metabolic Acidemia and Acute Kidney Injury: The BICARICU-2 Randomized Clinical Trial. JAMA, 334(22), 2000–2010. https://doi.org/10.1001/jama.2025.20231 (F)

[161] Sorohan, B. M., Obrișcă, B., Jurubiță, R., Lupușoru, G., Achim, C., Andronesi, A., Frățilă, G., Berechet, A., Micu, G., & Ismail, G. (2024). Sodium citrate versus sodium bicarbonate for metabolic acidosis in patients with chronic kidney disease: A randomized controlled trial. Medicine, 103(10), e37475. https://doi.org/10.1097/md.0000000000037475 (F)

[162] Jaber, S., Paugam, C., Futier, E., Lefrant, J.-Y., Lasocki, S., Lescot, T., Pottecher, J., Demoule, A., Ferrandière, M., Asehnoune, K., Dellamonica, J., Velly, L., Abback, P.-S., de Jong, A., Brunot, V., Belafia, F., Roquilly, A., Chanques, G., Muller, L., … BICAR-ICU Study Group. (2018). Sodium bicarbonate therapy for patients with severe metabolic acidaemia in the intensive care unit (BICAR-ICU): a multicentre, open-label, randomised controlled, phase 3 trial. The Lancet, 392(10141), 31-40. https://doi.org/10.1016/s0140-6736(18)31080-8 (A) Tuzatish nashri: https://doi.org/10.1016/S0140-6736(18)33040-X.

[163] Buyse, C., Joudiou, N., Corbet, C., Feron, O., Mignion, L., Flament, J., & Gallez, B. (2021). Impact of Inhibition of the Mitochondrial Pyruvate Carrier on the Tumor Extracellular pH as Measured by CEST-MRI. Cancers, 13(17), 4278. https://doi.org/10.3390/cancers13174278 (F)

[164] Page, M. J., McKenzie, J. E., Bossuyt, P. M., Boutron, I., Hoffmann, T. C., Mulrow, C. D., Shamseer, L., Tetzlaff, J. M., Akl, E. A., Brennan, S. E., Chou, R., Glanville, J., Grimshaw, J. M., Hróbjartsson, A.,

Lalu, M. M., Li, T., Loder, E. W., Mayo-Wilson, E., McDonald, S., … Moher, D. (2021). The PRISMA 2020 statement: An updated guideline for reporting systematic reviews. BMJ, 372, n71. https://doi.org/10.1136/bmj.n71

[165] Whiting, P. F., Tomlinson, E., Rutjes, A. W. S., Davenport, C. F., Yang, B., Westwood, M. E., Takwoingi, Y., Reitsma, J. B., Hyde, C., Bossuyt, P. M. M., Deeks, J. J., Leeflang, M. M. G., & Mallett, S. (2026). QUADAS-3: A revised tool for the quality assessment of diagnostic test accuracy studies. Annals of Internal Medicine, 179(4), 548–555. https://doi.org/10.7326/ANNALS-25-02104

[166] Schünemann, H. J., Higgins, J. P., Vist, G. E., Glasziou, P., Akl, E. A., Skoetz, N., & Guyatt, G. H. (2024). Chapter 14: Completing Summary of findings tables and grading the certainty of the evidence. In J. P. T. Higgins et al. (Eds.), Cochrane Handbook for Systematic Reviews of Interventions (version 6.5; chapter updated August 2023). Cochrane. https://www.cochrane.org/authors/handbooks-and-manuals/handbook/current/chapter-14

[167] Maintz, D., Heindel, W., Kugel, H., Jaeger, R., & Lackner, K. J. (2002). Phosphorus-31 MR spectroscopy of normal adult human brain and brain tumours. NMR in Biomedicine, 15(1), 18–27. https://doi.org/10.1002/nbm.735 (A)

[168] Korzowski, A., Weinfurtner, N., Mueller, S., Breitling, J., Görke, S., Schlemmer, H.-P., Ladd, M. E., Paech, D., & Bachert, P. (2020). Volumetric mapping of intra- and extracellular pH in the human brain using $^{31}$P MRSI at 7T. Magnetic Resonance in Medicine, 84(4), 1707–1723. https://doi.org/10.1002/mrm.28255 (F)

[169] Mürdter, T. E., Friedel, G., Backman, J. T., McClellan, M., Schick, M., Gerken, M., Bosslet, K., Fritz, P., Toomes, H., Kroemer, H. K., & Sperker, B. (2002). Dose optimization of a doxorubicin prodrug (HMR 1826) in isolated perfused human lungs: Low tumor pH promotes prodrug activation by beta-glucuronidase. Journal of Pharmacology and Experimental Therapeutics, 301(1), 223–228. https://doi.org/10.1124/jpet.301.1.223 (A)

[170] Toft, N. J., Axelsen, T. V., Pedersen, H. L., Mele, M., Burton, M., Balling, E., Johansen, T., Thomassen, M., Christiansen, P. M., & Boedtkjer, E. (2021). Acid-base transporters and pH dynamics in human breast carcinomas predict proliferative activity, metastasis, and survival. eLife, 10, e68447. https://doi.org/10.7554/eLife.68447 (F)

[171] Voss, N. C. S., Kold-Petersen, H., Henningsen, M. B., Homilius, C., & Boedtkjer, E. (2019). Upregulated $Na^+/H^+$-exchange protects human colon cancer tissue against intracellular acidification. BioMed Research International, 2019, 3702783. https://doi.org/10.1155/2019/3702783 (F)